國立臺灣大學工學院土木工程學系

碩士論文

Department of Civil Engineering

College of Engineering

National Taiwan University

Master's Thesis

地工泡棉加勁土壤受爆炸荷載之數值分析

Numerical analysis of geofoam reinforced soil subjected to blast loads

吳文崤

WEN-YAN WU

指導教授：楊國鑫 博士

Advisor: Kuo-Hsin Yang, Ph.D.

中華民國 113 年 7 月

July 2024

doi:10.6342/NTU202401573

摘要

地表爆炸所產生之壓力波會對地下結構物之安全造成威脅，本研究進行一系列數值模擬以探討地工泡棉加勁土壤於爆炸荷載下之動態行為與爆震波衰減機制。本研究之數值模型可分為未加勁砂土及地工泡棉加勁砂土兩種模型，模型中以 150 公斤 TNT 炸藥於土層表面引爆，並於炸藥引爆點距地表 3 公尺處之土層量測模型估計之土壤壓力及垂直加速度值。比較加入地工泡棉前後之土壤壓力與垂直加速度值，可發現土壤中之尖峰爆壓值衰減 60.77%、最大垂直加速度衰減 83.24%。本研究經過參數敏感性研究確認地工泡棉之爆壓衰減機制主要依賴地工泡棉與周圍土壤之波阻抗差。此外，本研究針對地工泡棉之建構方法(泡棉種類、泡棉厚度與泡棉埋設深度)進行了參數研究以探討地工泡棉加勁土壤於尖峰爆壓衰減性能最佳化之設計。參數研究結果顯示，隨地工泡棉密度增加、泡棉厚度與埋設深度提升時，土壤中之尖峰爆壓將有顯著衰減，尖峰爆壓之衰減最大可達 80.09%，最大垂直加速度衰減則可達到 96.97%。本研究基於數值模擬研究成果，提供了地工泡棉加勁土壤受爆炸載重時之量化分析流程與設計建議，可做為未來地下結構物進行防爆性能提升或設計時之參考選項之一。

關鍵字：數值模擬、爆炸荷載、地工合成材料、地工泡棉、波阻抗

doi:10.6342/NTU202401573

ABSTRACT

Pressure waves generated by surface explosions pose a significant threat to the safety of underground structures. This research conducted a series of numerical simulations to investigate the dynamic behavior of geofoam-reinforced soil under blast loads and the blast attenuation mechanism of geofoam-reinforced soil. The numerical models in this research are divided into two types: unreinforced and reinforced. In both models, 150 kg of TNT explosives are detonated on the surface of the soil layer. The blast pressure and vertical acceleration are measured 3 m below the ground surface at the point of detonation.

The results show that, with geofoam reinforcement, the peak blast pressure is reduced by 60.77%, and the peak vertical acceleration is reduced by 83.24%. This confirms that the blast attenuation mechanism of geofoam-reinforced soil is based on the difference in wave impedance between soil and geofoam.

Additionally, parametric studies were conducted to investigate the effects of various geofoam parameters (type, thickness, and embedded depth) on blast attenuation. The results indicate that as the density, thickness, and embedded depth of the geofoam increase, the protection effectiveness also increases. Specifically, the study found an

doi:10.6342/NTU202401573

80.09% reduction in peak blast pressure and a 96.97% reduction in peak vertical acceleration within the scope of this research.

Based on the numerical results, this research provides a quantified research procedure and design recommendations for geofoam-reinforced soil subjected to blast loads, offering valuable guidance for the future design of blast-resistant underground structures.

KEYWORDS: Numerical simulation, blast load, geosynthetics, geofoam, wave impedance

doi:10.6342/NTU202401573

TABLE OF CONTENTS

doi:10.6342/NTU202401573

doi:10.6342/NTU202401573

LIST OF TABLES

doi:10.6342/NTU202401573

LIST OF FIGURES

doi:10.6342/NTU202401573

doi:10.6342/NTU202401573

doi:10.6342/NTU202401573

Chapter 1. Introduction

1.1. Motivation

When underground structures such as air raid shelters, tunnels, and ammunition depots are subjected to blast waves released from weapon detonations, the covering soil acts as an attenuation material, dissipating the energy and reducing damage to the structures. Improving the resistance of underground structures against surface explosions hinges on the energy attenuation efficiency of the covering soil. In this context, reinforcing soil with geosynthetics emerges as a promising solution.

The geosynthetic-reinforced soil (GRS) structures have seen a wide application in civil engineering. Compared to conventional rigid reinforced concrete (RC) structures, GRS structures are more flexible and capable of withstanding larger deformations before failure. This characteristic makes GRS structures suitable for resisting lateral forces or shock loads from natural disasters. Figure 1-1 to Figure 1-3 shows a comparison of open-cut tunnels using geosynthetics and recycled tires as rockfall protections. As shown in Figure 1-3, the tunnel with recycled tire cover is heavily damaged after rockfall events, whereas the geosynthetic reinforced tunnel shown in Figure 1-2 remains intact.

doi:10.6342/NTU202401573

Apart from resisting natural disasters, GRS structures are used by the military as barriers against projectiles and explosions due to their shock load-resisting characteristics. For example, the HESCO bastion (shown in Figure 1-4), is a barrier consisting of wire mesh-reinforced geosynthetics filled with soil. It is commonly used to reduce the impact of shock waves from projectiles and explosives. Geosynthetic reinforcement enables the soil to dissipate energy from explosive detonations more effectively by providing additional tensile strength and preventing direct contact between the shock wave and the soil, thereby impeding stress transmission.

To enhance the protection of personnel and assets sheltered in underground structures against explosions, this research aims to investigate the effectiveness of geosynthetic-reinforced soil in attenuating blast waves, with a specific focus on geofoam-reinforced soil. Geofoam, due to its low density, low construction cost, and relatively high strength compared to soil, is considered an ideal material for reinforcing the soil in the blast attenuation layer.

doi:10.6342/NTU202401573

Figure 1-1 Open-cut tunnels with EPS (Expanded Polystyrene) foam covered on top for rockfall protection.

Figure 1-2 Open-cut tunnels with EPS foam cover after rockfall events.

doi:10.6342/NTU202401573

Figure 1-3 Open-cut tunnels with recycled tire cover collapsed after rockfall events. (SET News)

Figure 1-4 Barriers consist of HESCO bastions (Forbes, 2023)

doi:10.6342/NTU202401573

1.2. Research Objectives

In this research, the finite element program LS-DYNA is utilized to construct numerical models for explosives detonating on the surface of a soil layer. The objectives of this research are:

1. Investigate the soil layer's reaction when subjected to blast loads of surface detonation.

2. Investigate the geofoam's effectiveness as blast attenuation material by comparing soil's dynamic behavior under blast load with/without geofoam reinforcement.

3. Conduct parametric studies to understand the factors influencing geofoam's performance on shock wave attenuation.

4. Based on the aforementioned results, design recommendations for underground facilities' shock wave attenuation layer are proposed.

1.3. Research Outline

This thesis consists of 6 chapters (see Figure 1-5). The contents of each chapter are shown as follows:

Chapter 1: Introduction of the research motivation, background, and objectives.

doi:10.6342/NTU202401573

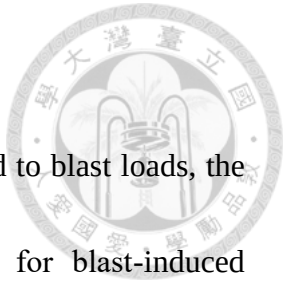

Chapter 2: Literature reviews on soil's behavior when subjected to blast loads, the geofoam's mechanism for wave attenuation, and the evaluation for blast-induced damages.

Chapter 3: Introduction to LS-DYNA numerical program, this research's model outline, and the model constitutive laws and parameters used in this research.

Chapter 4: Model validations for soil and geofoam's numerical modes and sensitivity studies on geofoam's protection performance.

Chapter 5: Evaluation of soil's behavior for unreinforced and reinforced ground, and the parametric studies on the geofoam-reinforced shock wave attenuation layer.

Chapter 6: Conclusions and recommendations based on the results of this research.

doi:10.6342/NTU202401573

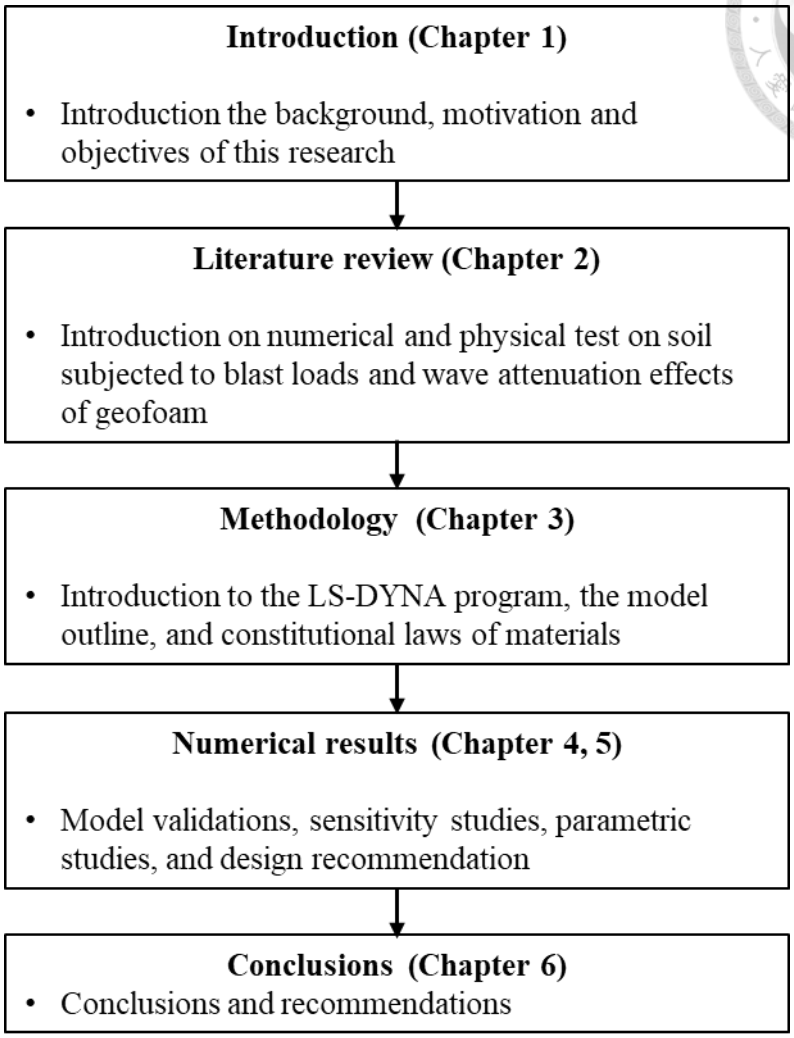

Figure 1-5 Overall scope and corresponding chapters in this thesis

doi:10.6342/NTU202401573

Chapter 2. Literature review

In this chapter, literature reviews were conducted. The following contents will be divided into three parts: soil's reaction when subjected to surface blast load, the wave attenuation effects of geofoam, and the evaluation of blast-induced damages.

2.1. Soil Behaviors Under Blast Loads

United States Army Corps of Engineers (USACE) conducted a series of tests on how explosions affect soil behaviors and developed several empirical equations for predicting soil behavior under the influence of shockwaves induced by explosive detonation. In the aforementioned empirical equations, the effects of soil types, moisture content, and soil particle sizes…etc. are taken into consideration. In design manual TM 5-855-1 proposed by USACE, there are a total of 20 soil models (as shown in Table 2-1) that vary from wet clay to crushed limestone to consider soil's dynamic behaviors under designated conditions.

doi:10.6342/NTU202401573

To estimate the soil's behavior under blast load, there are several equations proposed, this thesis will focus on the soil's stress estimation. The TM 5-855-1 manual lists the estimation of soil's stress under blast load in Eq.(2-1).

$$\sigma_p(r) = \frac{S_1}{r^{n_s}}(1+\frac{S_2}{r^2}) \tag{2-1}$$

where σ_p is the peak radial stress in soil, S_1 is the peak stress coefficient, S_1 is the peak stress coefficient, n_s is the peak stress decay constant, *r* is the straight-line distance from the explosive's center of gravity to the point of interest.

In Eq.(2-1), the explosive is assumed to be 1kg of H-6 explosive, to consider differences in explosive power, explosive mass, and locations of detonation, parameters S_1, and S_2 are scaled based on the aforementioned conditions. S_1, S_2 are scaled in accordance with Eq.(2-2) and Eq.(2-3):

$$S_1^{'} = S_1(W_{\exp losive}E_f C_f)^{\frac{n_s}{3}} \tag{2-2}$$

$$S_2^{'} = S_2(W_{\exp losive}E_f C_f)^{\frac{2}{3}} \tag{2-3}$$

where $S_1^{'}$ and $S_2^{'}$ are the scaled peak stress coefficient, $W_{\exp losive}$ is the mass of the explosive, E_f is the equivalent mass factor (see Table 2-2), and C_f is the coupling factor (see Figure 2-1).

doi:10.6342/NTU202401573

Table 2-1 Material model name and properties proposed in TM 5-855-1 manual: (a) Basic properties; (b) Peak stress coefficients (U.S. D.A., 1998)

(a) Basic properties

Model name	Description	Specific gravity, G_s	Dry density, γ_d (t/m^3)	Water content ω (%)	Porosity (%)	Saturation (%)
DEMODRY_1	Dry Sand	2.67	1.69	4	30	18.3
DEMOWET_1	Wet Clay	2.71	1.59	24.8	3	92.6
ICLAY_1	Gravelly Clay	2.71	1.71	15.8	9.9	73.2
WCALY_2	Plastic Clay	2.71	1.59	23.7	3.9	90.6
WCALY_3	Plastic Clay	2.75	1.42	34.1	0	100
WCALY_4	Plastic Clay	2.75	1.42	33.4	1	97.9
WCALY_5	Clayey Sand	2.75	1.42	30.5	5	89.7
ISOL	Clayey Sand	2.72	1.8	12.1	12	64.5
DSOIL3	Plaster Sand	2.69	1.85	2.5	26.5	15.1
DSOIL4	Concrete Sand	2.69	1.85	5.2	25.7	12.6
DSOIL2	Concrete Sand	2.7	1.79	4	26.5	21.4
WSOIL_1	Concrete Sand	2.7	1.79	18.8	0	100
WSOIL_2	Concrete Sand	2.7	1.79	18.2	1	97
WSOIL_3	Crushed Sandstone	2.7	1.79	16	5	85.2
IROCK_1	Crushed Sandstone	2.63	1.72	12.9	12.5	63.9
IROCK_2	Crushed Pumice	2.15	0.85	28.6	36	40.2
IROCK_3	Crushed Limestone	2.79	2.26	3.5	11.1	41.6
WROCK_1	Crushed Limestone	2.79	2.26	8.4	0	100
WROCK_2	Crushed Limestone	2.79	2.26	7.9	1	94.7
WROCK_3	Crushed Limestone	2.79	2.26	6.2	5	73.7

doi:10.6342/NTU202401573

(b) Peak stress coefficients

Model name	Type	Peak stress coefficient, S_1 (MP$a-m^{n_S}$)	Peak stress coefficient, S_2 (MP$a-m^{n_S}$)	Peak stress decay constant n_s n_s
DEMODRY_1	Dry Sand	2.17	0.137	1.57
DEMOWET_1	Wet Clay	4.08	0	2.54
ICLAY_1	Gravelly Clay	2.14	0.091	2.2
WCALY_2	Plastic Clay	4.08	0	2.54
WCALY_3	Plastic Clay	56.33	0	1.25
WCALY_4	Plastic Clay	7.52	0	2.8
WCALY_5	Clayey Sand	3.76	0.152	1.75
ISOL	Clayey Sand	1.5	0.122	2.2
DSOIL3	Plaster Sand	1.4	0.046	2.1
DSOIL4	Concrete Sand	1.66	0.205	1.7
DSOIL2	Concrete Sand	1.94	0.091	1.8
WSOIL_1	Concrete Sand	3.74	0	1.3
WSOIL_2	Concrete Sand	3.74	0	3.2
WSOIL_3	Crushed Sandstone	1.67	0.198	2
IROCK_1	Crushed Sandstone	2.89	0.061	2
IROCK_2	Crushed Pumice	0.81	0	2.3
IROCK_3	Crushed Limestone	2.58	0.061	2
WROCK_1	Crushed Limestone	61.94	0	1.3
WROCK_2	Crushed Limestone	4.48	0	3.2
WROCK_3	Crushed Limestone	2.3	0.122	2.1

doi:10.6342/NTU202401573

Table 2-2 Equivalent mass factors for explosives

Explosive	Equivalent mass factor, E_f
H-6	1.00
PETN-1.8	0.98
C-4	0.96
Composition A-3	0.92
ANFO-0.82	0.90
ANFO-0.85	0.90
Cyclotol (77/23)	0.90
Octol (78/22)	0.90
Composition B, Grade A	0.85
Pentolite	0.81
Tetryl	0.76
TNT	0.73

doi:10.6342/NTU202401573

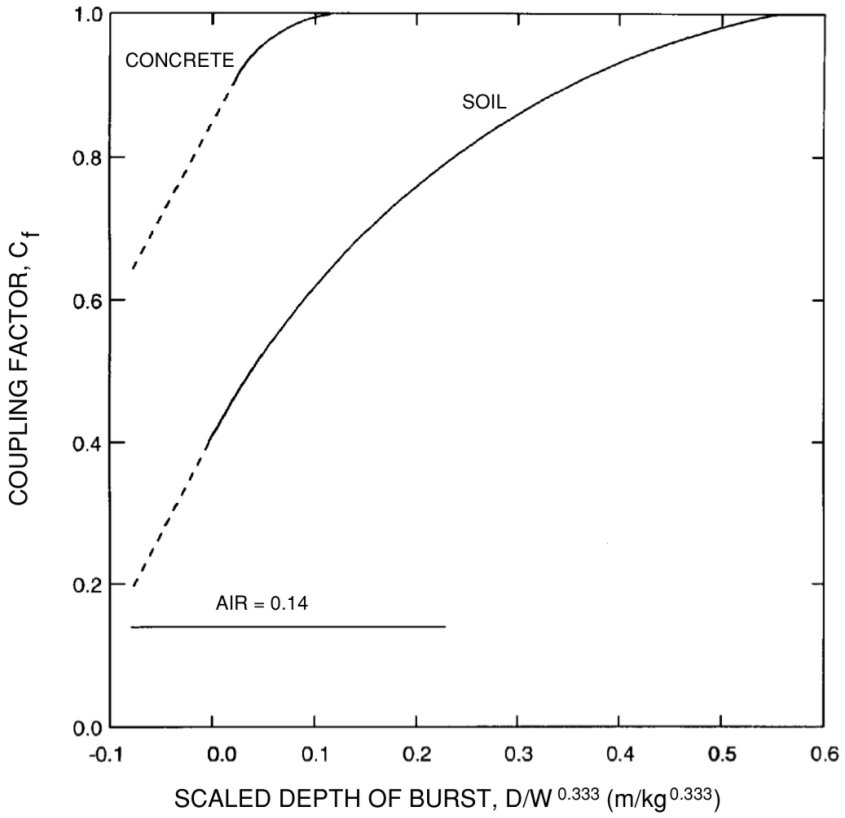

Figure 2-1 Ground shock coupling factor for burst in air, soil, and concrete (U.S. D.A., 1998)

doi:10.6342/NTU202401573

Tseng et al. (2022) conducted experiments and numerical simulations to investigate the sandy soil's behavior under surface explosion and the effects of non-woven geotextile reinforcements on the reduction of soil blast pressure, as shown in Figure 2-2. In this research, numerical models can successfully replicate the pressure-time history and the shell crater measured in field experiments. Also, the field experiments found out that sandy soil reinforced with non-woven geotextile can reduce the blast-induced soil stress through tension membrane effect. When geotextile-reinforced soil is subjected to external loads such as blast loads, geotextiles can provide the soil with extra tensile strength to resist external forces, as shown in Figure 2-3.

doi:10.6342/NTU202401573

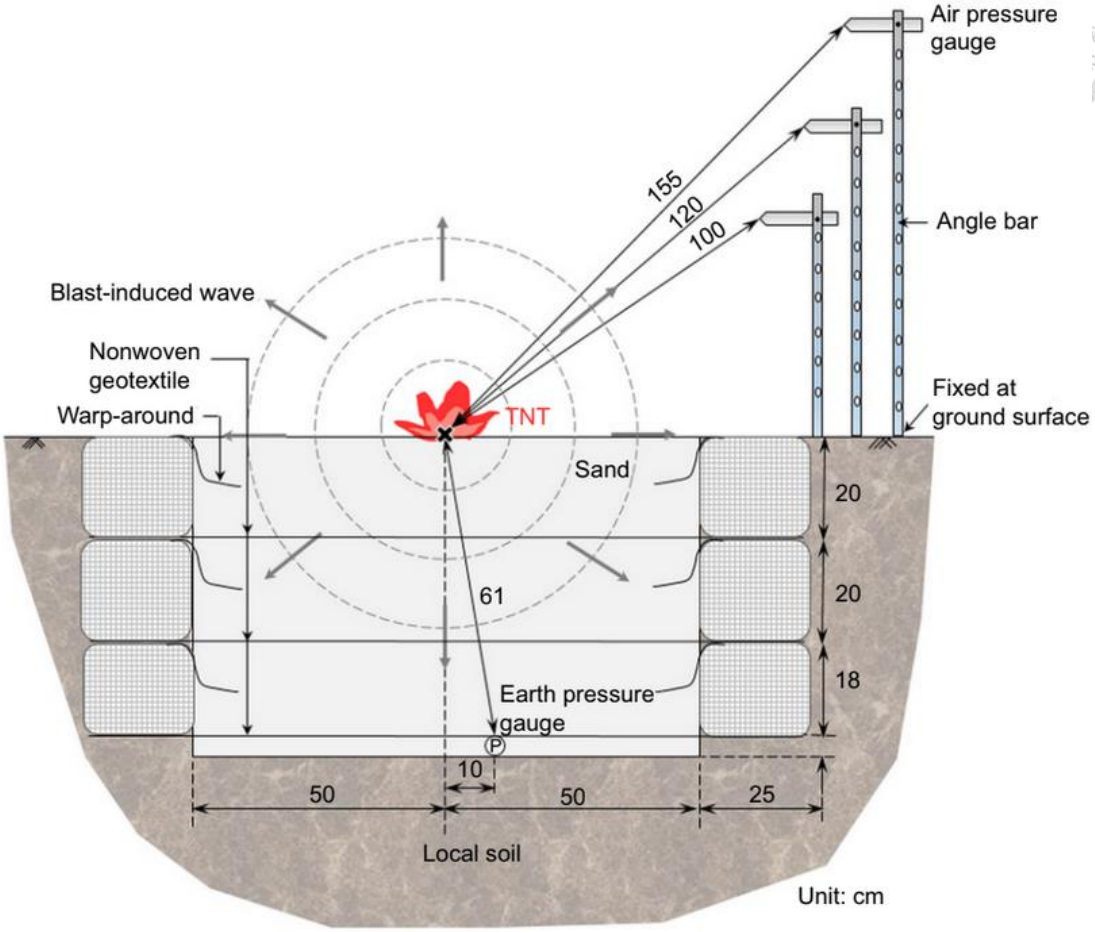

Figure 2-2 Explosion test layout (Tseng et al., 2022)

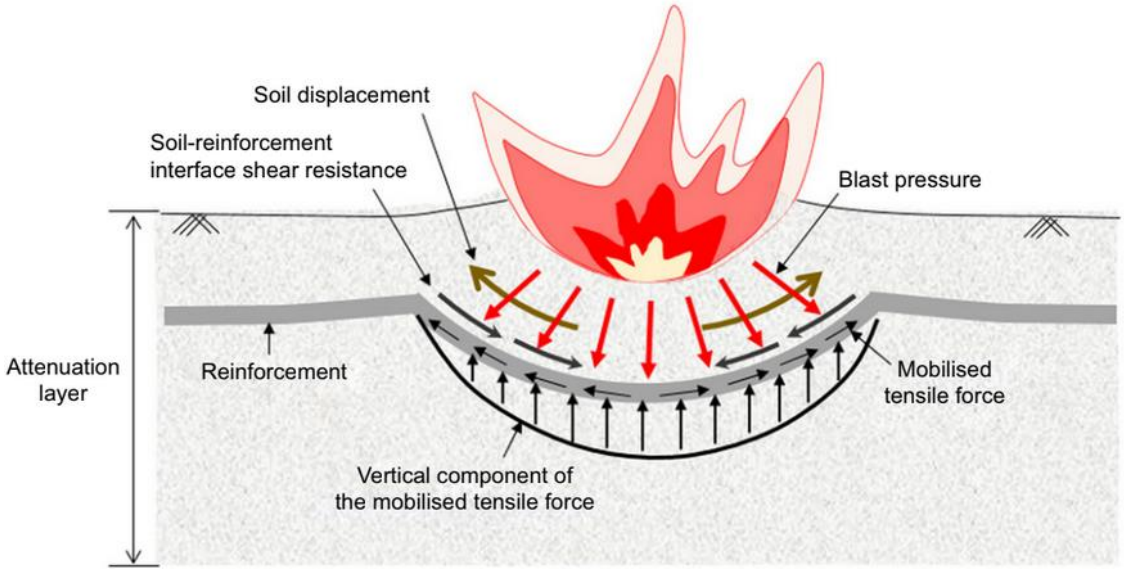

Figure 2-3 Reinforcing mechanism of geotextile-reinforced soil (Tseng et al., 2022)

doi:10.6342/NTU202401573

Busch et al. (2016) conducted experiments and numerical simulations to evaluate clayey soil's behavior under explosive air blasts (Figure 2-4, Figure 2-5). This research used numerical software LS-DYNA to simulate the air blast experiments. The soil was simulated with LS-DYNA material 147: FHWA_SOIL model, which is based on the Mohr-Coulomb constitutive law to describe the soil's stress-strain behaviors. The numerical results indicate that the FHWA_SOIL model can effectively predict the shell crater generated by air blast. Similarly, Lee (2006) conducted numerical simulations to describe the blast-induced soil liquefaction with the LS-DYNA program's FHWA_SOIL model. In this research, detailed parametric studies were conducted to evaluate the theoretical and physical meaning of each model parameter. Lee (2006) found that with the FHWA_SOIL model, the change in soil's pore water pressure and porosity can be correctly modeled.

Also, other researchers such as Jayasinghe et al. (2013), Dubec et al. (2018), and Linforth et al. (2019) conducted similar research to describe the soil's behavior under blast loads.

doi:10.6342/NTU202401573

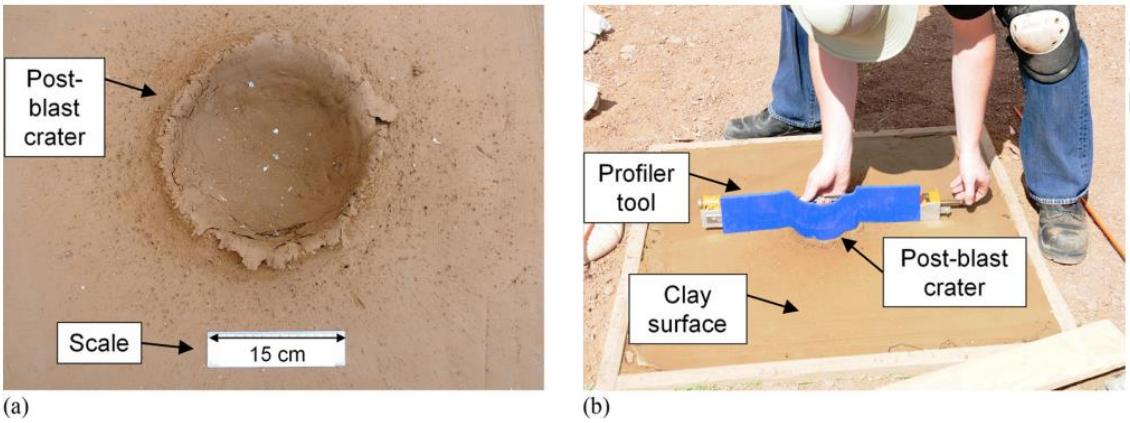

Figure 2-4 (a) Air blast-induced shell crater formed on clayey soil (b) Measurement of shell crater (Busch et al., 2016)

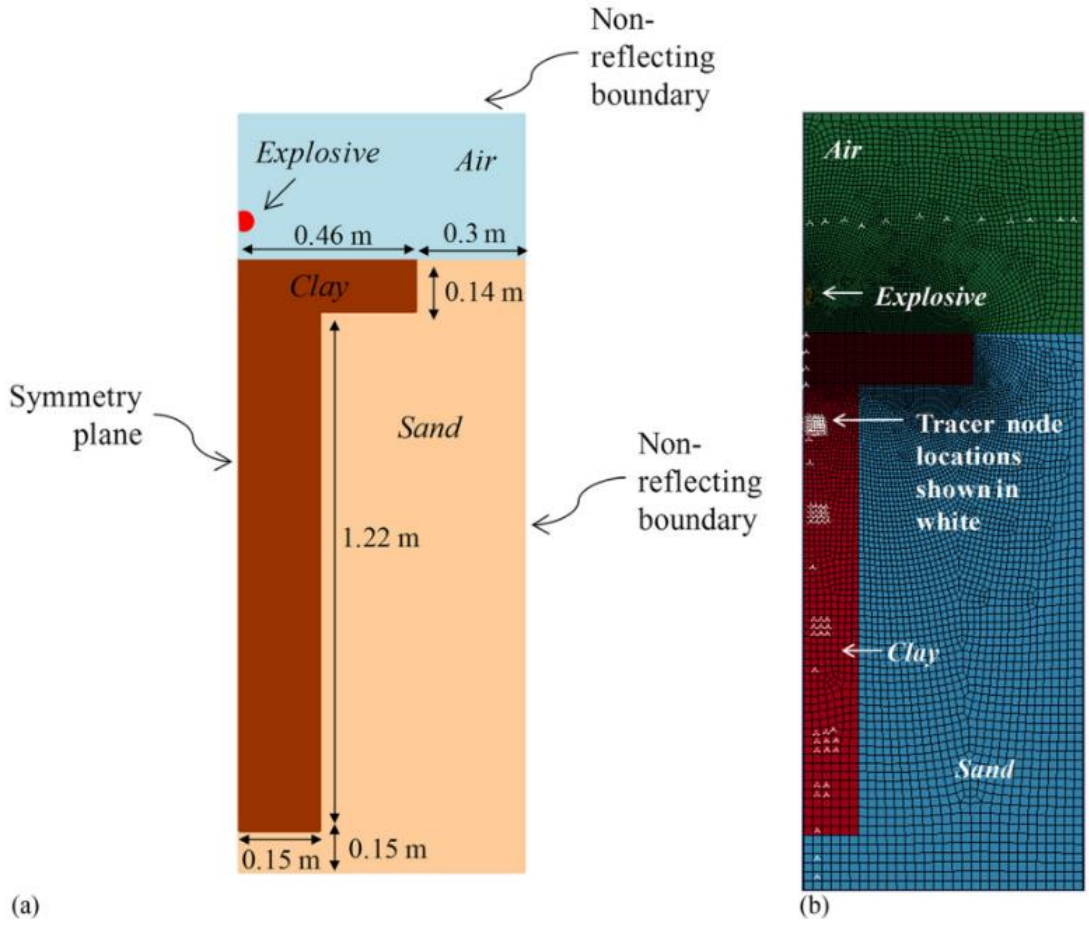

Figure 2-5 (a) Geometry and boundary condition for numerical simulation (b) Numerical model for air blast experiments (Busch et al., 2016)

doi:10.6342/NTU202401573

2.2. Wave Attenuation Effects of Geofoam

In Woods' (1968) research, it was found that excavating trenches near either the source of vibration or its receiver can effectively isolate the vibration (see Figure 2-6). Based on this finding, it is suggested that by installing low-density materials in the ground, vibratory wave transmission would be impeded, leading to the isolation of ground shocks.

Wang (2009) and Barman et al. (2023) conducted numerical simulations on geofoam's performance as wave barriers for vibration and explosions. Through their research, it is proposed that the low-density materials' wave isolation mechanism is based on the wave impedance difference between the soil and barrier materials (i.e. air in excavated trenches and geofoams). The wave impedance is estimated with Eq.(2-4):

$$Z = \rho V \tag{2-4}$$

where Z is the wave impedance, ρ is the material's density, and V represents the velocity of the wave to propagate in the material, in terms of the blast attenuation, V represents the pressure wave velocity. Wave impedance represents the resistance for a wave to experience when passes through certain media, higher wave impedance indicates a higher energy loss during transmission. Once passing through media with different

doi:10.6342/NTU202401573

wave impedances, energy losses would occur at the material interface, leading to the isolation of waves (Wang, 2009).

De et al. (2015) used centrifuge tests to examine the protection effectiveness of geofoam-reinforced subterranean pipelines when subjected to blast loads (see Figure 2-7). Through the experiments, it is found that with geofoam protection, the axle strain measured on the top of the underground pipeline is significantly reduced. Indicating the geofoam's potential to serve as reinforcements for underground structures.

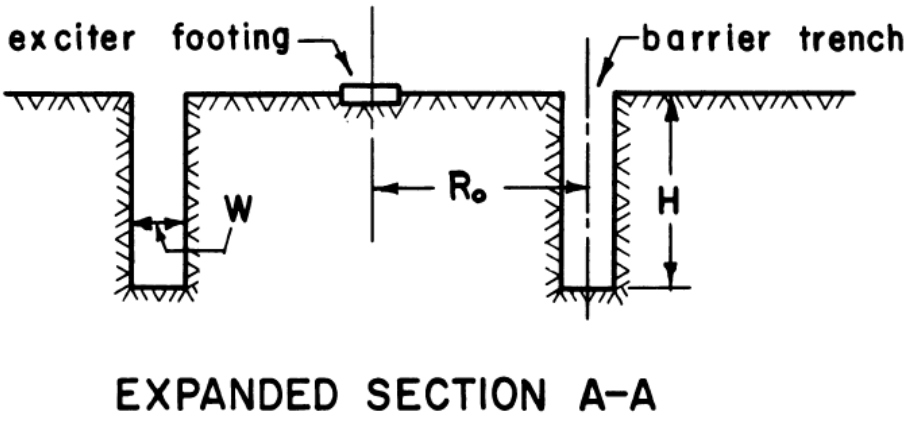

Figure 2-6 Vibration isolation test setup (Woods, 1968)

doi:10.6342/NTU202401573

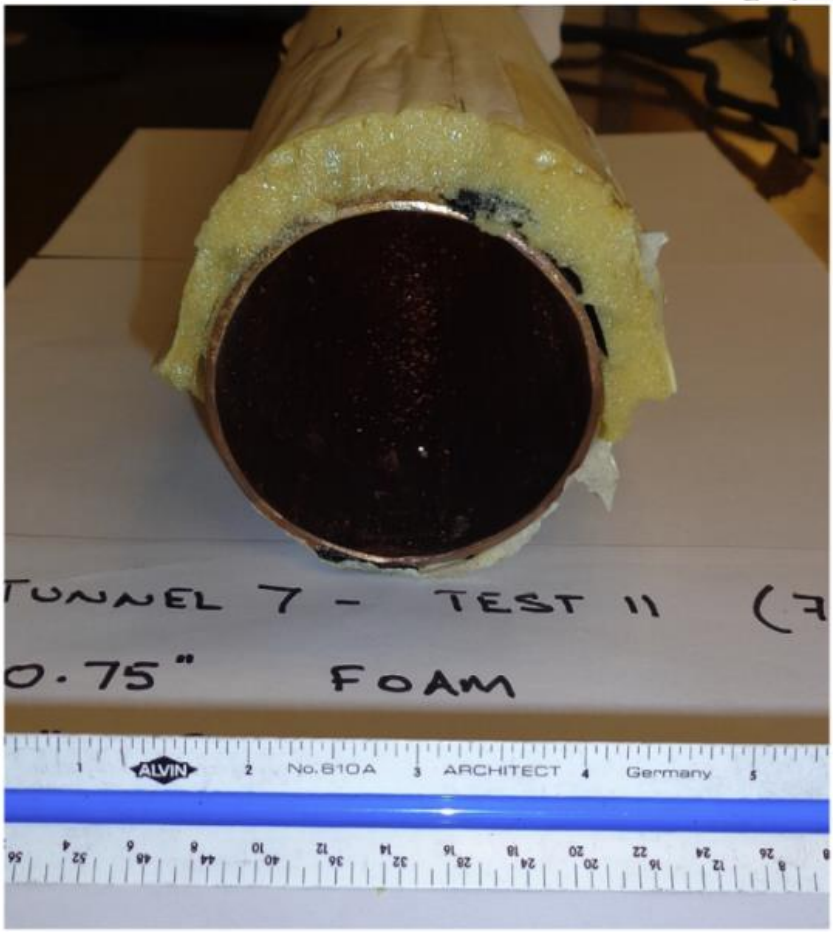

Figure 2-7 The underground pipelines with protective geofoam barrier (De et al., 2015)

doi:10.6342/NTU202401573

Chapter 3. Numerical Study Program

In this study, a series of numerical analyses are performed to investigate the response of the unreinforced and reinforced soil under blast load. In this chapter, the analysis program used in this research and material models used are introduced.

3.1. Introduction of the LS-DYNA Program

In this study, the LS-DYNA program Version 11.0 was deployed to conduct numerical simulations on soil's dynamic behavior under blast loads.

LS-DYNA is a finite element analysis program that was developed in the 1970s by Dr. John O. Hallquist at Lawrence Livermore National Laboratory (LLNL). Originally created due to a lack of software at LLNL for carrying out three-dimensional stress analysis for weapon development, LS-DYNA is capable of performing stress analysis of structures under various loadings such as explosion, impact, and more. This allows the analysis of the non-linear stress-strain behavior of structures and materials (LS-DYNA, 2022).

To estimate the large deformation of structures induced by severe impact, LS-DYNA is equipped with multiple description methods: Lagrangian, Eulerian, coupled

doi:10.6342/NTU202401573

Lagrangian-Eulerian, and arbitrary Lagrangian-Eulerian (ALE) descriptions. In Lagrangian description, materials are attached to the coordinate grids. As the materials deform due to external forces, the material mesh deforms correspondingly. However, severe deformations can cause significant distortions in mesh, leading to difficulties in calculation or even termination of calculation. In contrast, the Eulerian description, allows materials to flow freely through the mesh, meaning the coordinate grids do not deform with the materials. While the Eulerian description avoids mesh distortion problems present in the Lagrangian description, defining boundary conditions becomes challenging because the materials are not constrained within mesh (LS-DYNA, 2005; Tseng et al., 2022).

An ALE description combines the advantages of both Lagrangian and Eulerian descriptions, making it possible to obtain the stress-strain behaviors of materials under severe forces. The time step of an ALE description is as follows (LS-DYNA, 2022):

1. **Perform a Lagrangian time step:** When the mesh is distorted, it is smoothed and remapped to ensure model stability while maintaining boundary condition mesh nodes unchanged.

doi:10.6342/NTU202401573

2. **Perform an advection time step:** After distortion, changes within the mesh, such as material density, and stress, are updated according to the node's velocity vector for the next time step's calculation, the visualized ALE time step is shown in Figure 3-1.

Since this research focuses on the soil's dynamic behavior under blast loads, considering the massive distortion and impacts caused by explosive detonation, conducting simulations under the ALE description would be an appropriate choice to achieve the research objectives.

doi:10.6342/NTU202401573

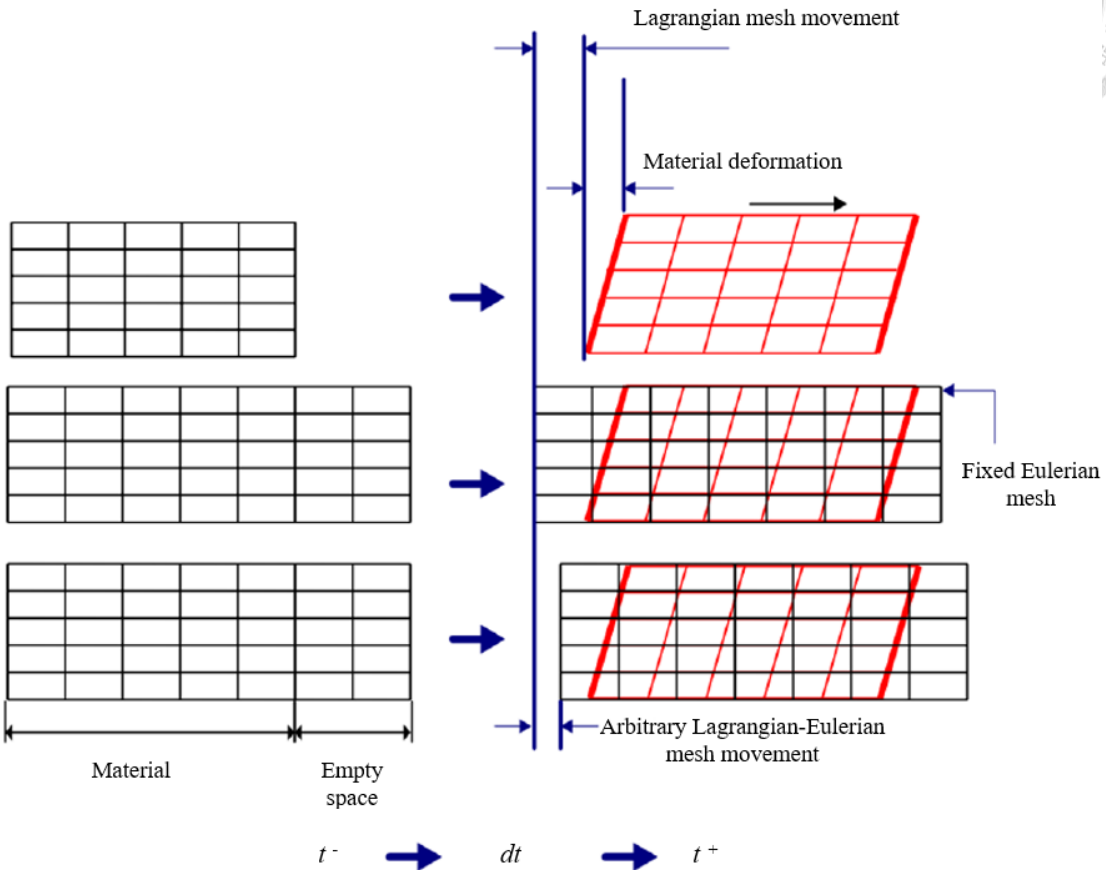

Figure 3-1 Time steps of arbitrary Lagrangian-Eulerian description (Zhao, 2003)

3.2. Numerical Model and Convergence Analysis

Figure 3-2 illustrates a general layout of an underground shelter as proposed in the United States Army design manual TM 5-855-1. The protection of an underground shelter mainly relies on two components: an anti-penetration layer and a shock wave attenuation layer. The anti-penetration layer, typically made of reinforced concrete or rubbles, resists the incoming projectiles and prevents damage to the protected structure. The shock

doi:10.6342/NTU202401573

wave attenuation layer, generally composed of sandy soil backfills, dissipates the energy of blast waves from weapon detonations.

Since the focal point of this research is enhancing the energy dissipation effectiveness of the attenuation layer, the basic assumption of the numerical model is that the incoming projectile penetrates the anti-penetration layer and detonates on top of the blast attenuation layer. The assumed explosive mass is 150 kg of trinitrotoluene (TNT) dynamite. In terms of energy release, detonation of 1 g of TNT would release an energy of $4.184\times10^{3} J$. For 150 kg of TNT, the energy output during detonation is estimated to be $6.276\times10^{8} J$.

To reduce model complexity, the anti-penetration layer and the underground structure are not considered in the numerical model. This approach assumes the missile penetrates the anti-penetration layer and reaches and explodes at the top of the attenuation layer. The thickness of the blast attenuation layer is assumed to be 3 m, and the peak blast pressure in soil will be measured at the same depth below the explosive's detonation center.

Two numerical models are considered in this study: unreinforced ground and reinforced soil. The general outline for these two categories is similar: a field with

doi:10.6342/NTU202401573

dimensions of 10 m × 5 m × 10 m (length × depth × height) as shown in Figure 3-3 ~ Figure 3-6. To reduce the required calculation time, only half of the model is constructed, with reflective boundary conditions set on the symmetric plane (X-Z plane). Apart from the symmetric plane, the other model boundaries are set to be non-reflective boundaries to prevent the reflection of blast waves.

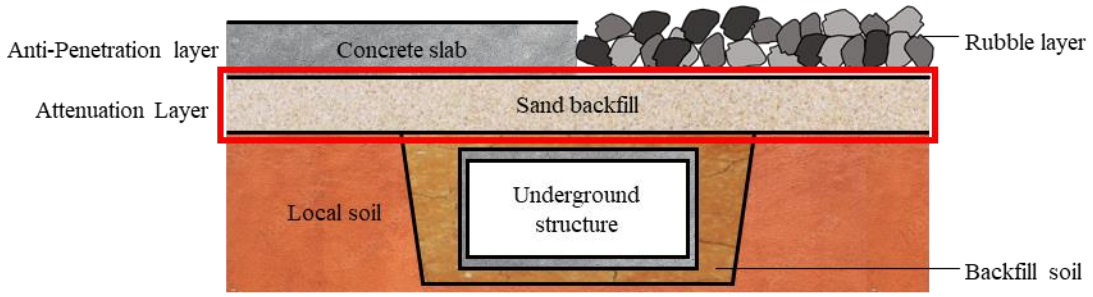

Figure 3-2 General layout of underground structure recommended by US Army manual TM 5-855-1

doi:10.6342/NTU202401573

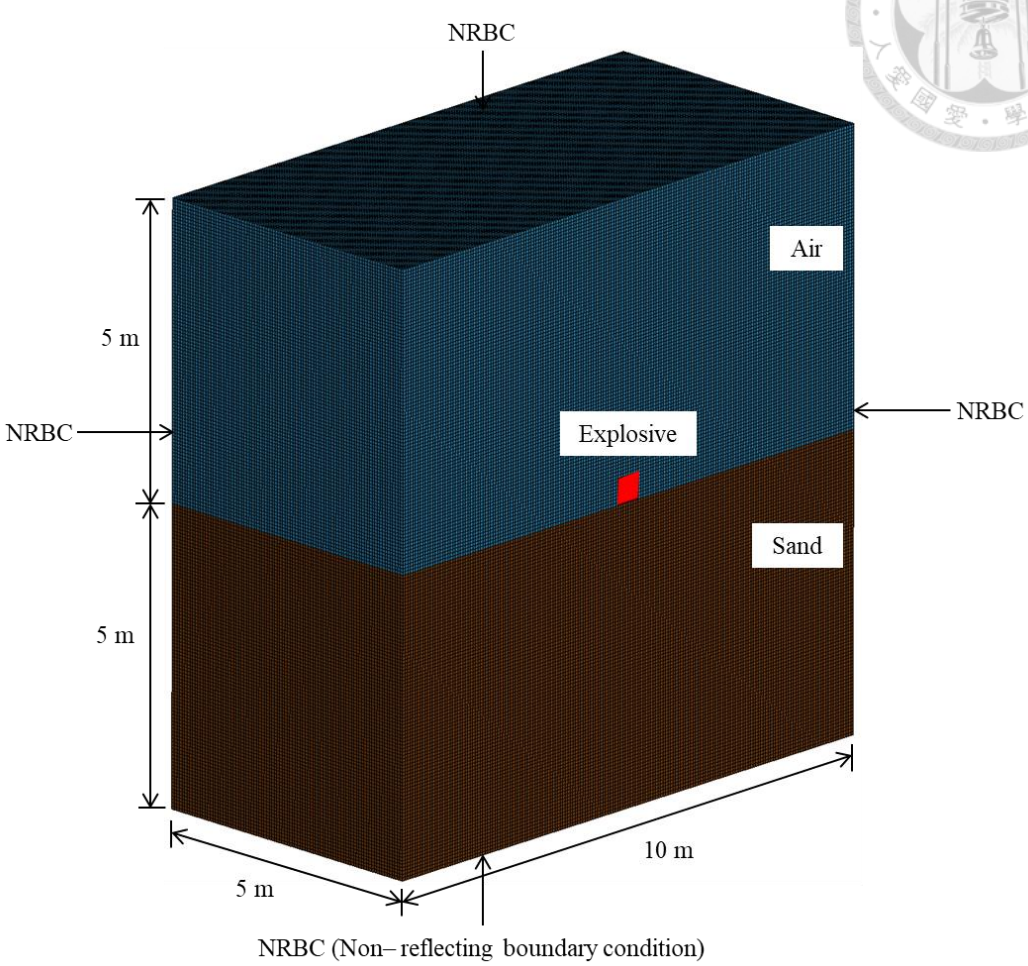

Figure 3-3 Model outline of full-scale numerical model for unreinforced ground

doi:10.6342/NTU202401573

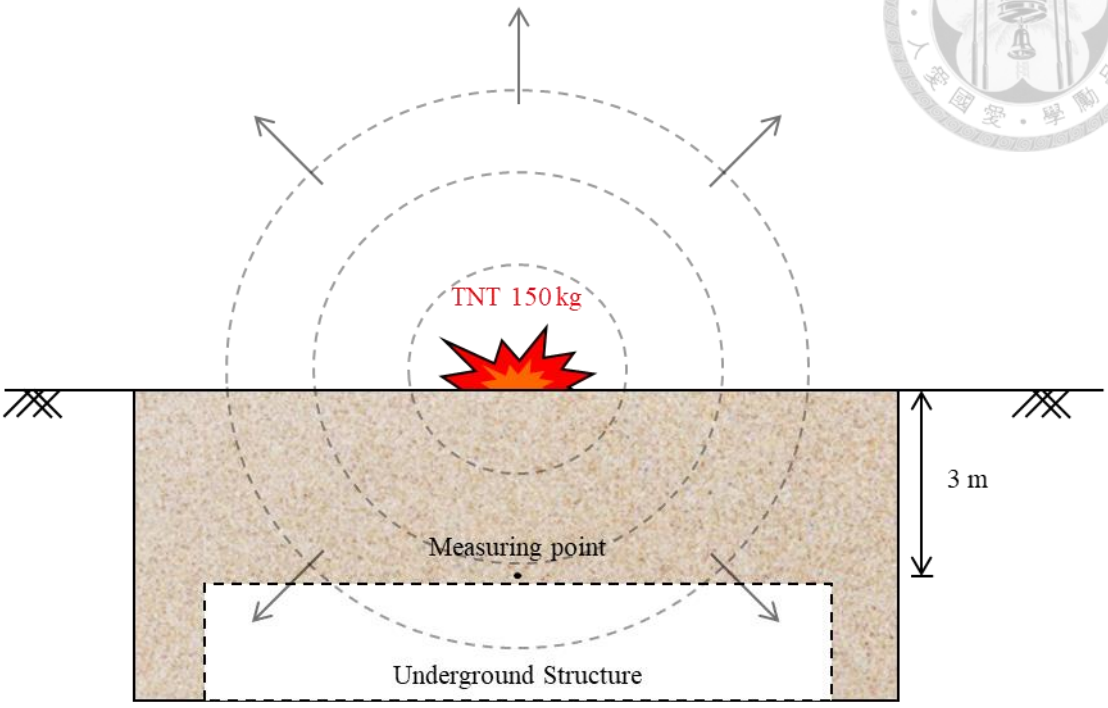

Figure 3-4 Schematic diagram of full-scale numerical model for unreinforced ground

doi:10.6342/NTU202401573

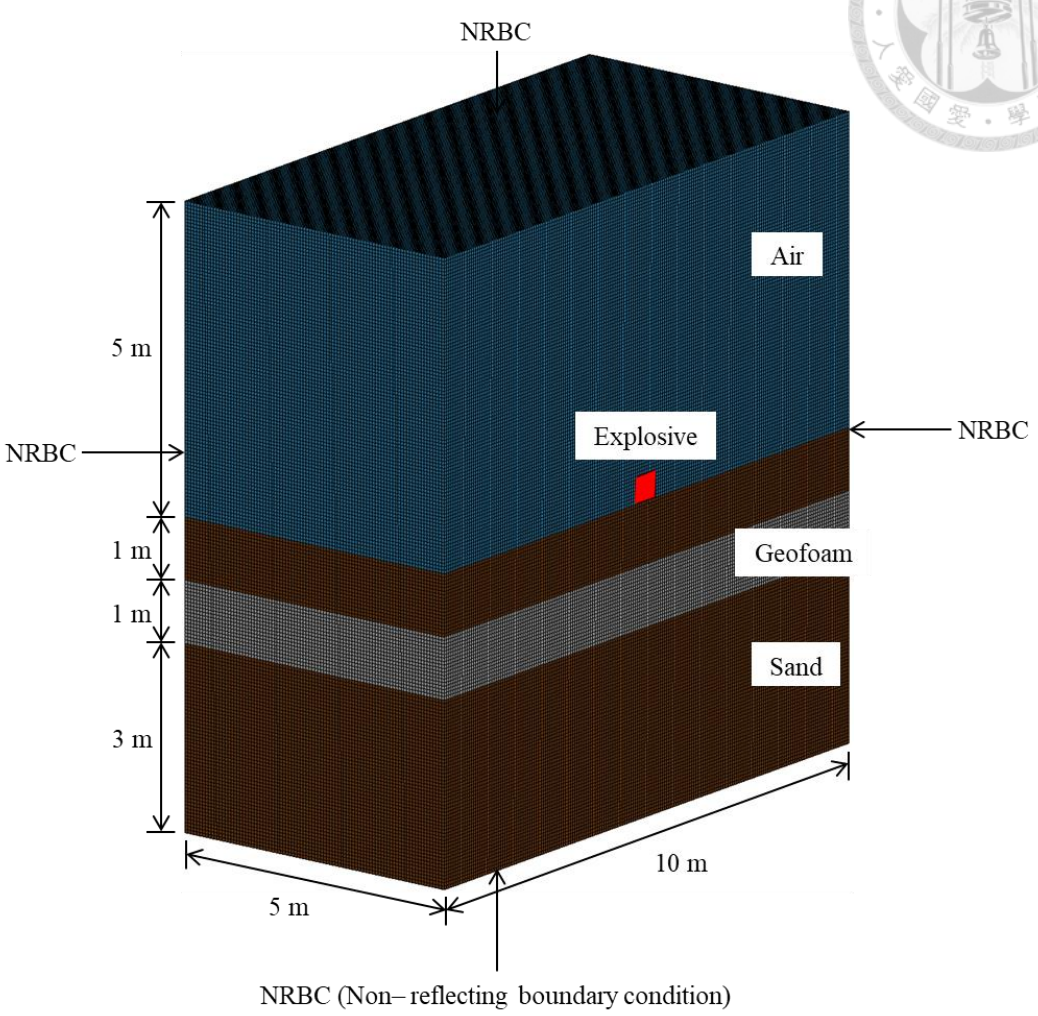

Figure 3-5 Model outline of full-scale numerical model for reinforced ground

doi:10.6342/NTU202401573

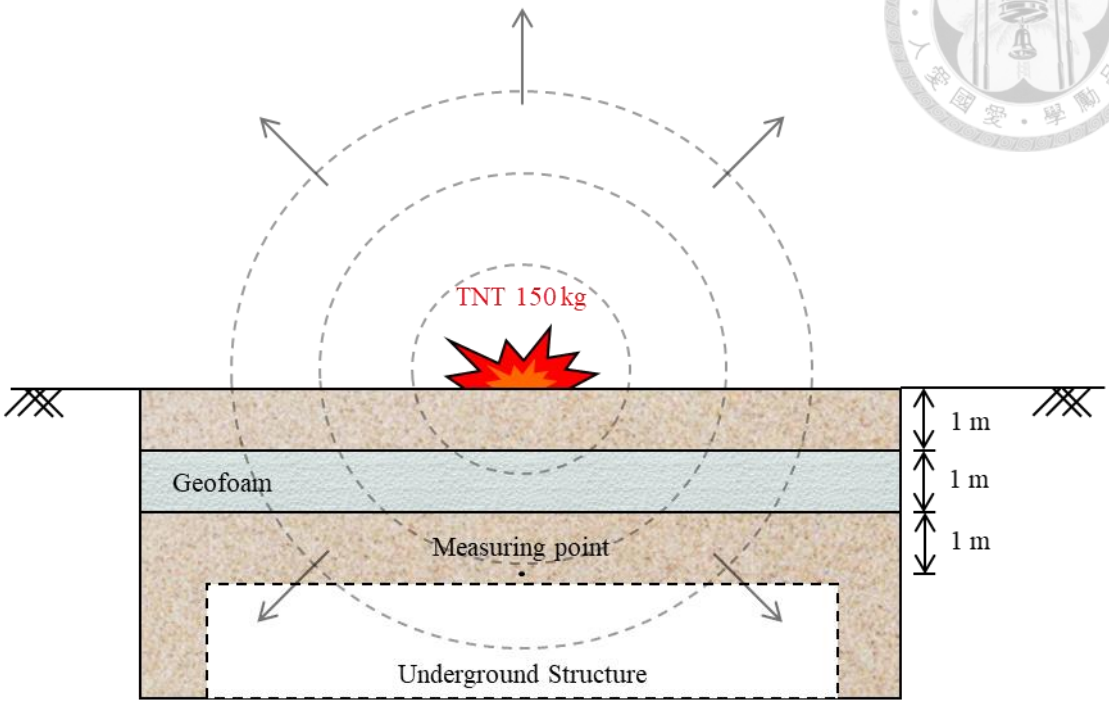

Figure 3-6 Schematic diagram of full-scale numerical model for unreinforced ground

doi:10.6342/NTU202401573

To determine the suitable mesh size for numerical models, convergence analysis was conducted. Four models with different mesh sizes were constructed: 22.57 cm, 11.29 cm, 5.64 cm, and 4.52 cm. The number of elements in each models are: 42,592, 340,736, 2,916,000 ,and 5,324,000. The numerical results for convergence analysis are shown in Table 3-1 and Figure 3-7. Figure 3-7 indicates as soil depth increases, the peak blast pressure in soil converges. Comparing the differences in peak blast pressure 3 m below ground surface and the required calculation time, it is observed that the difference in P_b is quite small, without exceeding the 10% range. However, the time of calculation needed changed significantly, ranging from 44 seconds to over 20 hours. Based on the numerical results, the mesh size of 5.64 cm is determined. Compared to other mesh sizes, it has a well convergence in peak blast pressure at 3 m below the ground surface while maintaining a relatively low calculation time.

Table 3-1 Results of convergence analysis

Mesh size (cm)	Element counts	P_b (MPa)	Difference in P_b compared to the previous model (%)	Calculation time
22.57	42,592	1.892	-	44 sec
11.29	340,736	2.010	5.90	6 hr
5.64	2,916,000	1.930	4.17	8 hr
4.52	5,324,000	1.962	1.61	20 hr

doi:10.6342/NTU202401573

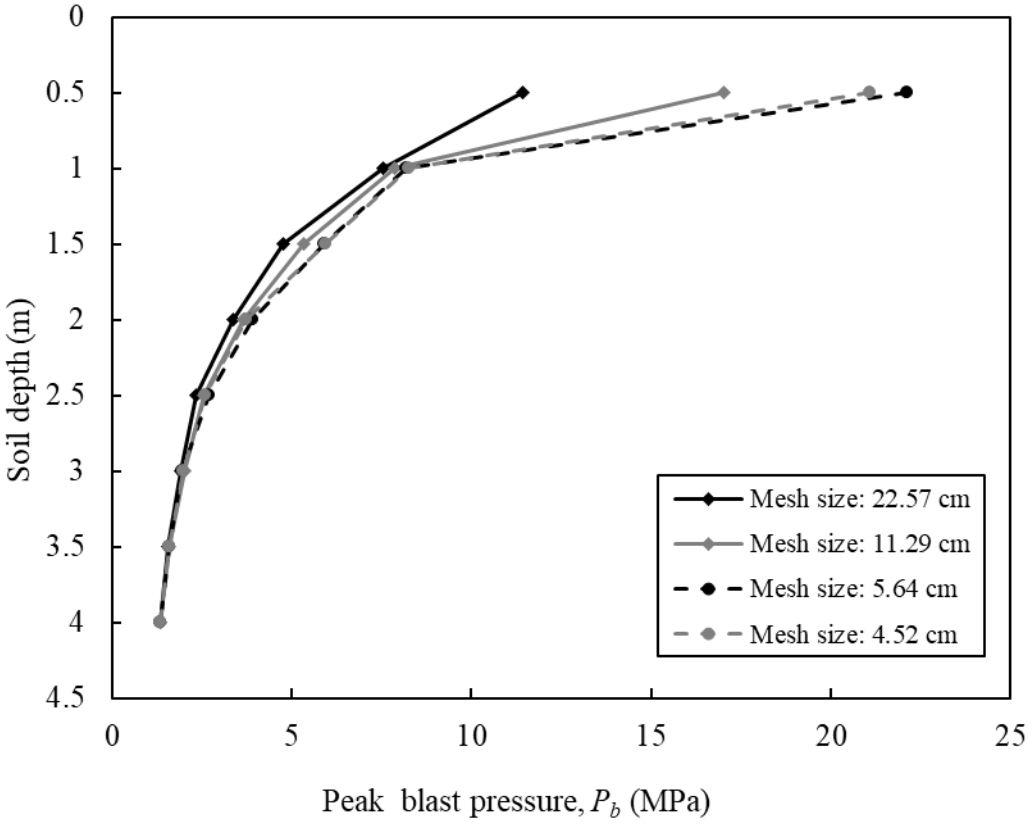

Figure 3-7 Convergence analysis on numerical model's mesh size

doi:10.6342/NTU202401573

3.3. Material Models and Input Properties

3.3.1. TNT

In this research, the simulation of TNT explosives is performed with LS-DYNA material model MAT_008 HIGH_EXPLOSIVE_BURN to simulate the shock wave transmitted through air and soil after detonation. The model parameters are referenced from the research conducted by Tseng et al. (2022). The input parameters required by the numerical model include density, detonation velocity, Chapman-Jouget pressure, and the explosive's equation of state. The equation of state for the explosive's description is shown as Eq.(3-1):

$$P = A(1-\frac{\omega}{R_2 V_r})e^{-R_1 V_r} + B(1-\frac{\omega}{R_1 V_r})e^{-R_2 V_r} + \frac{\omega E_0}{V_r} \quad (3\text{-}1)$$

where P is pressure, V_r is relative volume, E_0 represents initial internal energy. The input parameters used in this research are listed in Table 3-2.

doi:10.6342/NTU202401573

Table 3-2 Material properties of TNT (Tseng et al., 2022)

Material model			
Density ρ (kg/m^3)	Detonation velocity, V_D (m/s)	Chapman-Jouget pressure, (GPa)	
1630	6930	21	
Equation of state: JWL			
Parameter, A (GPa)	Parameter, B (GPa)	Parameter, R_1	Parameter, R_2
371	3.23	4.15	0.95
Initial internal energy (J/m^3)	Initial volume (m^3)		
6.99×10^9	1×10^{-6}		

3.3.2. Air

In the assumptions of this research, explosives are detonated on the ground surface, thus the effects of blast transmission in the air shall also be considered. According to Tseng et al. (2022), the behavior of air is described in the LS-DYNA program using the MAT_009 NULL material model and the LINEAR_POLYNOMIAL equation of state. The input parameters for this material model include density, dynamic viscosity and pressure cutoff. The equation of state describing air behavior is shown in Eq.(3-2) and Eq.(3-3).

doi:10.6342/NTU202401573

$$P = C_0 + C_1\mu + C_2\mu^2 + C_3\mu^3 + (C_4\mu + C_5\mu^2 + C_6\mu^3)E \quad (3\text{-}2)$$

$$\mu = \frac{\rho}{\rho_0} - 1 \quad (3\text{-}3)$$

where P is air pressure, E is internal energy per unit reference volume, $C_0 \sim C_6$ are polynomial equation coefficients, ρ is current air density, ρ_0 is initial air density. To simulate ideal gas, polynomial coefficients C_0, C_1, C_2, C_3, C_6 are recommended to be zero, and coefficient $C_4 = C_5 = \gamma - 1$, where γ is air's ratio of specific heats. (LS-DYNA, 2022)

Based on the recommended coefficient settings, the equation of state for ideal gas is given by Eq.(3-4):

$$P = (\gamma - 1)\frac{\rho}{\rho_0}E \quad (3\text{-}4)$$

The input parameters for air's numerical model are shown in Table 3-3.

doi:10.6342/NTU202401573

Table 3-3 Material properties of air (LS-DYNA, 2022; Tseng et al., 2022)

Material model			
Density ρ (kg/m^3)		Pressure cutoff, P_C (GPa)	Dynamic viscosity, M_U (kg/sm)
1.29		0	0
Equation of state: Linear polynomial			
Coefficient C_0, C_1, C_2, C_3, C_6	Coefficient C_4, C_5	Initial internal energy, E_0 (J/m^3)	Initial volume, V_0 (m^3)
0	0.4	3.22×10^5	1×10^{-6}

3.3.3. Soil

The soil constitutive law chosen for this research is the MAT_147 FHWA_SOIL model, first proposed by Lewis (1999) for the Federal Highway Administration. The model is developed based on the Mohr-Coulomb and Drucker-Prager yield criterion and also considers the effects of soil's void ratio and excess pore water pressure on soil stress-strain behaviors. The FHWA_SOIL model's description of soil under blast load has been validated in multiple research. Simulations on soil's dynamic behaviors such as soil liquefaction and compaction, have been proven accurate with this constitutive law (Lee, 2006; Jayasinghe, 2013; Busch, 2016; Dubec, 2018; Linforth, 2019).

doi:10.6342/NTU202401573

Compared to other soil models in LS-DYNA program (e.g., MAT_005 SOIL_AND_FOAM, MAT_016 PSEUDO_TENSOR), the FHWA_SOIL model requires several assumed parameters that are not accessible through common soil tests, their introduction and recommended values are described as follows. It shall be noted that this research focuses specifically on the simulation of sandy soil, so the recommended model parameters apply exclusively to sand.

Failure Surface

In the model description of LS-DYNA manual, the yield surface of FHWA_SOIL model is a hyperbolic fit to the Mohr-Coulomb surface, as shown in Eq.(3-5):

$$\sigma_y = -P\sin(\phi) + \sqrt{J_2 K(\theta)^2 + AHYP^2 \sin^2(\phi)} - c\cos(\phi) = 0 \quad (3\text{-}5)$$

where *P* is the mean soil stress, ϕ is the internal friction angle, J_2 is the second invariant of the stress deviator, *c* is the cohesion, and *AHYP* is the Drucker-Prager coefficient to determine how the yield surface is fitted to standard Mohr-Coulomb yield surface. According to parametric studies conducted by Reid et al. (2004), the range of coefficient *AHYP* is shown as Eq.(3-6):

$$0 \le AHYP \le \frac{c}{20}\cot(\phi) \quad (3\text{-}6)$$

doi:10.6342/NTU202401573

When *AHYP* = 0, shape of the yield surface is fitted to standard Mohr-Coulomb yield surface (see Figure 3-8). It is noted that, for cohesionless soil like sands, if the cohesion value equals zero, this may lead to premature failure of soil during simulation. Such a problem is due to the lack of confining stresses for near-surface soil. To prevent this situation from occurring, the model investigation carried out by Reid et al. (2004) suggested assigning a small amount of cohesion to cohesionless soil, preventing premature failure of soil elements. According to Reid, a cohesion value of 6 kPa is suitable to maintain model stability while preventing inaccuracies in simulation of the soil.

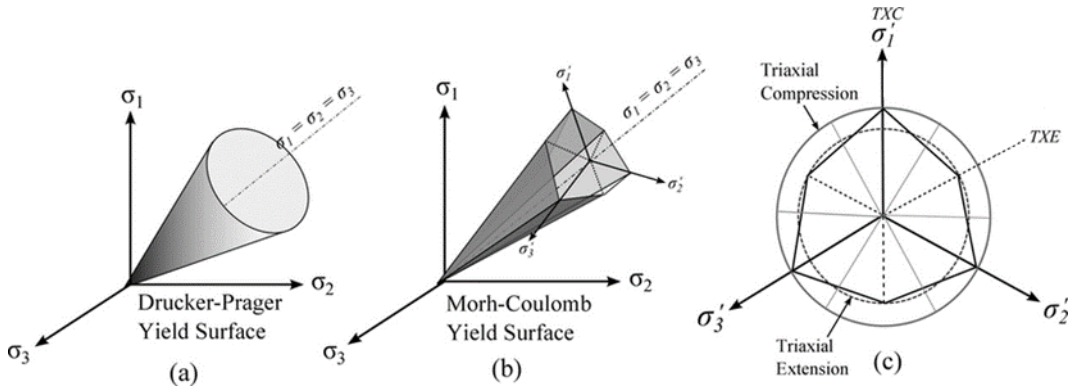

Figure 3-8 Yield surfaces under different failure criteria: (a) Drucker-Prager yield surface (b) Mohr-Coulomb yield surface (c) Drucker-Prager and Mohr-Coulomb yield surface on deviatoric plane (Garner et al., 2015)

doi:10.6342/NTU202401573

$K(\theta)$ is the function of the angle in the yield surface's deviatoric plane. The shape of the deviatoric plane, according to Klisinski (1985), is given as Eq.(3-7) and Eq.(3-8):

$$K(\theta) = \frac{4(1-e^2)\cos^2(\theta) + (2e-1)^2}{2(1-e^2)\cos(\theta) + (2e-1)\sqrt{4(1-e^2)\cos^2(\theta) + 5e^2 - 4e}} \tag{3-7}$$

$$\cos(3\theta) = \frac{3\sqrt{3}J_3}{2\sqrt{J_2{}^3}} \tag{3-8}$$

where J_3 is the third invariant of the stress deviator, and e (in the model parameters, it is described as *ECCN*) describes the ratio between soil's triaxle extension strength to triaxle compression strength, ranging from 0.55 to 1. If e equals 1, a standard conical Mohr-Coulomb yield surface is formed, while a triangular yield surface is formed when e equals 0.55. According to Reid et al. (2004), a value of 0.7 is recommended for sand.

Soil's Strain-Hardening Behavior

In the FHWA_SOIL model, to simulate soil's strain-hardening behavior, the friction angle of soil changes as its effective plastic strain increases. The relationship between effective plastic strain and friction angle is shown in Eq.(3-9):

$$\Delta\phi = E_t\left(1 - \frac{\phi - \phi_{\text{int}}}{A_n\phi_{\max}}\right)\Delta\varepsilon_{eff\_plastic} \tag{3-9}$$

doi:10.6342/NTU202401573

where $\Delta\phi$ is changes in friction angle, $\Delta\varepsilon_{eff\_plastic}$ is changes in effective plastic strain, A_n is the threshold for initiation of non-linear behavior, and E_t determines the rate of strain hardening. According to Reid et al. (2004), these two parameters have no experimental or theoretical method to determine appropriate values. Thus, based on the research of Jayasinghe (2013), Busch (2016), Dubec (2018), and Linforth (2019), A_n and E_t is recommended to be 0.25 and 0.01.

Pore Pressure's Effect on Soil

To simulate the soil's air and moisture's effect on soil behavior, the changes in bulk modulus are shown as Eq.(3-10):

$$K = \frac{K_i}{1 + K_i D_1 n_{cur}} \tag{3-10}$$

where K_i is the soil's initial bulk modulus, n_{cur} represents the soil's current porosity, D_1 is the soil stiffness factor before air voids in soil collapsed.

To calculate the soil's pore water pressure, a similar equation for estimating changes in bulk modulus is utilized:

$$u = \frac{K_{sk}}{1 + K_{sk} D_2 n_{cur}} \varepsilon_v \tag{3-11}$$

doi:10.6342/NTU202401573

where K_{sk} is the soil's bulk modulus without air voids (skeleton bulk modulus), D_2 is the soil's pore water pressure factor before air voids in soil are collapsed, and ε_v is the soil's total volumetric strain.

Based on Reid et al. (2004) and Lee (2006), parameter K_{sk} is recommended to be 1% ~ 20% of the soil's bulk modulus. In this research, 10% is selected. As for parameters D_1 and D_2, since the soil is assumed to be linear elastic and pore water pressure's effect on soil is not considered in this research, both two parameters are set to zero.

Maximum Number of Plasticity Iterations

Since the FHWA_SOIL model is developed based on a modified Mohr-Coulomb method to fit the yield surface. To approach the Mohr-Coulomb yield surface, an iterative approach is utilized. In the FHWA_SOIL model, the number if iterative calculations is controlled by parameter *ITERMAX*. Based on the parametric study carried out by Lee (2006), the recommended number of iterations is 10, which maintains a balance between the numerical model's accuracy and required computation time.

Strain Rate's Effects on Soil Behaviors

The model developer deploys a two-parameter algorithm into the soil model to consider the potential effect of rate-dependent behaviors of soil. The two-parameter

doi:10.6342/NTU202401573

algorithm deploys an interpolative calculation between the elastic trial stress and inviscid stress to obtain the viscoplastic stress as shown in Eq.(3-12) ~ Eq.(3-14):

$$\bar{\sigma}_{vp} = (1-\zeta)\bar{\sigma} + \bar{\sigma}_{trial} \tag{3-12}$$

$$\zeta = \frac{\eta}{\Delta t + \eta} \tag{3-13}$$

$$\eta = \left(\frac{\gamma_r}{\dot{\varepsilon}}\right)^{\frac{V_n - 1}{V_n}} \tag{3-14}$$

where $\bar{\sigma}_{vp}$ is the viscoplastic stress, $\bar{\sigma}$ is the inviscid stress, $\bar{\sigma}_{trial}$ is the elastic trial stress. Parameter γ_r (GAMMAR) and V_n (VN) control the viscoplastic behavior of soil, when γ_r is set to zero, the soil's strain rate-dependent behavior is disabled. Based on Jayasinghe (2013), Busch (2016), Dubec (2018), and Linforth (2019), γ_r and V_n are recommended to be 0.0001 and 2.

Fracture Energy and Initial Damage Threshold

Parameter *VDFM* and *DINT* represent the fracture energy and the volumetric strain required for soil failure, respectively. Fracture energy is the area under the softening region of the soil's stress-strain curve times the cube root of the soil element's volume. Based on parametric studies conducted by Reid et al. (2004), there is no experimental or theoretical method to determine the recommended values for *VDFM* and *DINT*. Based on

doi:10.6342/NTU202401573

Jayasinghe (2013), Busch (2016), Dubec (2018) and Linforth (2019), *VDFM* and *DINT* are recommended to be 1 and 0.15.

Element Deletion Threshold

Parameters *DAMLEV* and *EPSAMX* represent the level of damage that a soil element withholds before it is deemed to fail and excluded from the simulation. *DAMLEV* is the percentage of material damage for element deletion, whereas EPSMAX is the maximum volumetric strain before soil element deletion; during simulation, soil elements will not be deleted unless both of the criteria are met. However, according to Reid (2004), turning on element deletion will lead to instabilities in the simulation process, thus element deletion is recommended to be turned off for the sake of model stability. To turn off the element deletion function, *DAMLEV* should be set to zero. The model parameters used in this research are listed in Table 3-4, the soil tests were conducted by Tseng et al. (2022).

doi:10.6342/NTU202401573

Table 3-4 Model parameters for standard quartz sand

RO (kN/m^3)	*SPGRAV*	*RHOWAT* (kN/m^3)	V_n	γ_r
16.350	2.65	10	2	0.0001
ITERMAX	*K* (MPa)	*G* (MPa)	*PHIMAX* (deg)	*AHYP* (kPa)
10	22.10	10.2	37	0.462
COH (kPa)	*ECCEN*	A_n	E_t	*MCONT*
6	0.7	0.25	0.01	0
PWD_1 (MPa)	PWK_{SK} (MPa)	PWD_2 (MPa)	*PHIRES* (deg)	*DINT*
0	2.21	0	33	0.15
VDFM	*DAMLEV*	*EPSMAX*		
1	0	0		

doi:10.6342/NTU202401573

3.3.4. Geofoam

This section will discuss the constitutive law for geofoam and its model parameters. In this research, the material model for geofoam is MAT_005 SOIL_AND_FOAM, which is based on the constitutive model proposed by Krieg (1972). In Krieg's model, the yield function is described as:

$$f = J_2 - (a_0 + a_1 p + a_2 p^2) \tag{3-15}$$

where a_0, a_1 and a_2 are material constants, J_2 is the second invariant of deviatoric stress, p is the mean stress. The application of this model requires input of the modeled material's stress-strain curve. Once the compressive volumetric strain exceeds the input data, stress is calculated using the following equation:

$$S_{ij}^{n+1} = \sqrt{(\frac{a_0 + a_1 p + a_2 p^2}{J_2})} S_{ij} \tag{3-16}$$

This research uses three types of EPS geofoam, EPS 15, EPS 22 and EPS 39 in simulation. The model parameters are listed in Table 3-5. The model parameters are referenced from the research of Khodaparast et al. (2022) and the American Society for Testing and Materials' standard specifications on geofoam (ASTM D6817).

doi:10.6342/NTU202401573

Table 3-5 Geofoam parameters for SOIL_AND_FOAM model:

(a) Input parameters (b) Stress-strain curve

(a)Input parameters

EPS type	Density, γ (kN/m^3)	Young's modulus E (MPa)	Poisson ratio v	Bulk modulus K (MPa)	Shear modulus G (MPa)	Compressive resistance at 1% strain (kPa)
EPS 15	0.144	2.48	0.09	1.14	1.00	25
EPS 22	0.212	5.03	0.13	2.23	2.25	50
EPS 39	0.384	10.34	0.22	4.24	6.14	75

(b) Stress-strain curve

Geofoam type	Stress, σ (kPa)									
EPS 15	0.000	2.305	7.575	13.503	19.432	24.290	30.038	45.367	62.723	90.439
EPS 22	0.000	4.510	14.818	26.415	38.011	47.514	58.759	88.745	122.695	176.911
EPS 39	0.000	8.575	28.174	50.223	72.273	90.341	111.722	168.735	233.285	336.369
Strain, ε	0.000	0.021	0.086	0.200	0.300	0.400	0.442	0.507	0.540	0.559

doi:10.6342/NTU202401573

Chapter 4. Model Validations and Sensitivity Studies

This chapter presents the model validation results. In the model validation, the numerical results obtained in this study are compared with the experiment test results for the unreinforced soil case and compared with the numerical results from the past study for the reinforced case. Additionally, sensitivity studies are conducted to identify the governing parameter for the blast attenuation performance of geofoam.

4.1. Model Validations

In this section, a series of validations are conducted to ensure the accuracy of the numerical model and its settings. The model validation is divided into two parts: the first validates the numerical models for soil. The second part validates the numerical models for geofoam.

4.1.1. Validation of Soil's Numerical Model

To validate the soil model used in this research, a numerical model was constructed based on the field explosion tests conducted by Tseng et al. (2022). The numerical model is shown in Figure 4-1. To reconstruct the field experiment conducted by Tseng et al. (2022), a soil field with a width of 2 m and a depth of 1 meter is constructed. The

doi:10.6342/NTU202401573

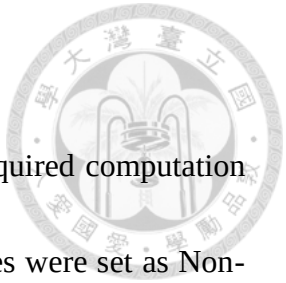

numerical model is symmetric along the X-Z plane to reduce the required computation time. Apart from the symmetric plane, all the other model boundaries were set as Non-reflecting boundaries to absorb the blast wave.

Compared to the field experiment, the numerical model is twice as wide as the sand pit used in the research by Tseng et al. (2022). This decision was made to eliminate the possible reflecting stress waves stemming from the model boundary's proximity to the stress measuring point. To ensure the accuracy of the numerical model, the soil's hydrostatic pressure was measured at a depth of 58 cm, with a 10 cm offset from the center of detonation, consistent with the field experiment's configuration. The schematic diagram is shown in Figure 4-2.

The validation results are shown in Figure 4-3. Comparing the numerical results with the pressure gauge reading from the field experiment, it can be observed that the blast wave's time of arrival in both pressure-time curves is similar. Both curves reached their peak at t = 1 ms. However, the second peak in soil blast pressure observed in the field experiment does not appear in the numerical model. The discrepancy is likely due to the expanded model dimensions, which were intended to eliminate the effects of model boundaries.

doi:10.6342/NTU202401573

When comparing the peak blast pressure measured in soil, the numerical model predicted a peak pressure of 502 kPa, which has a 6.98 % error compared to the 539 kPa measured in the field test. The numerical results indicate a successful replication of the sandy soil used in Tseng's research, thereby validating the soil model used in this research.

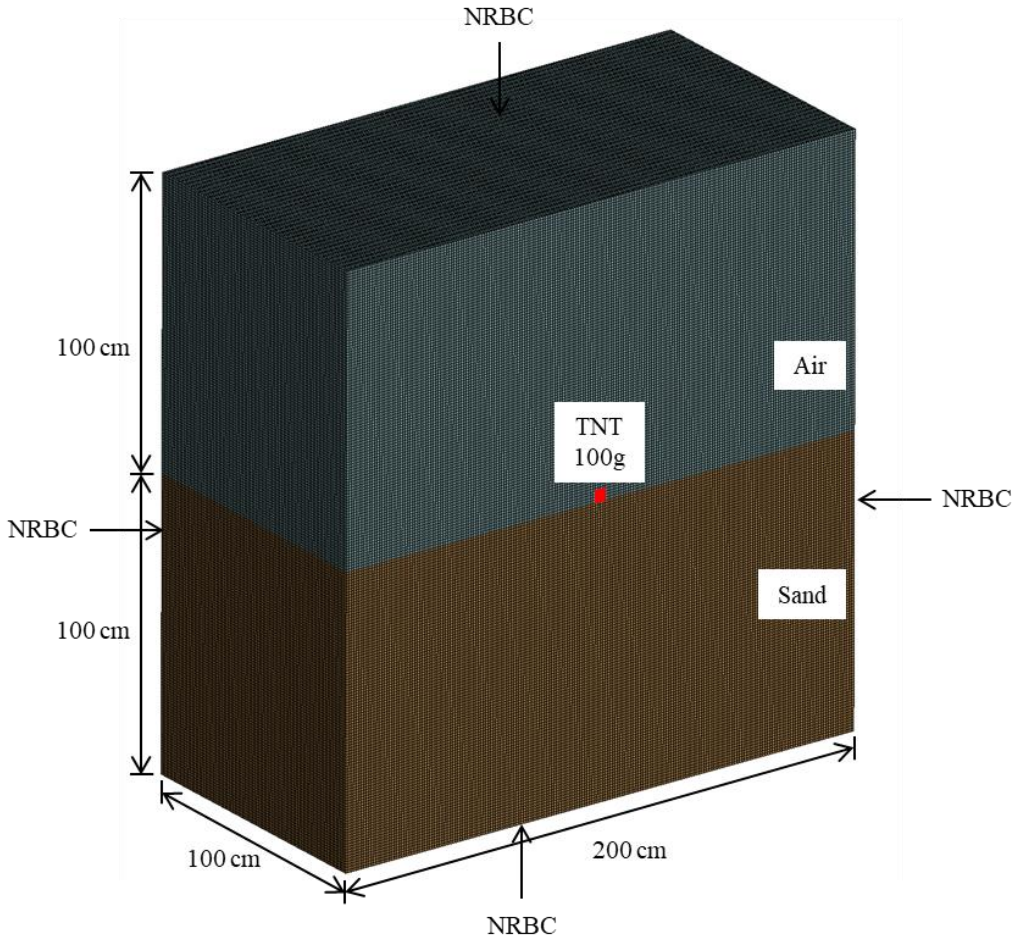

Figure 4-1 Numerical model for validation of soil model parameters

doi:10.6342/NTU202401573

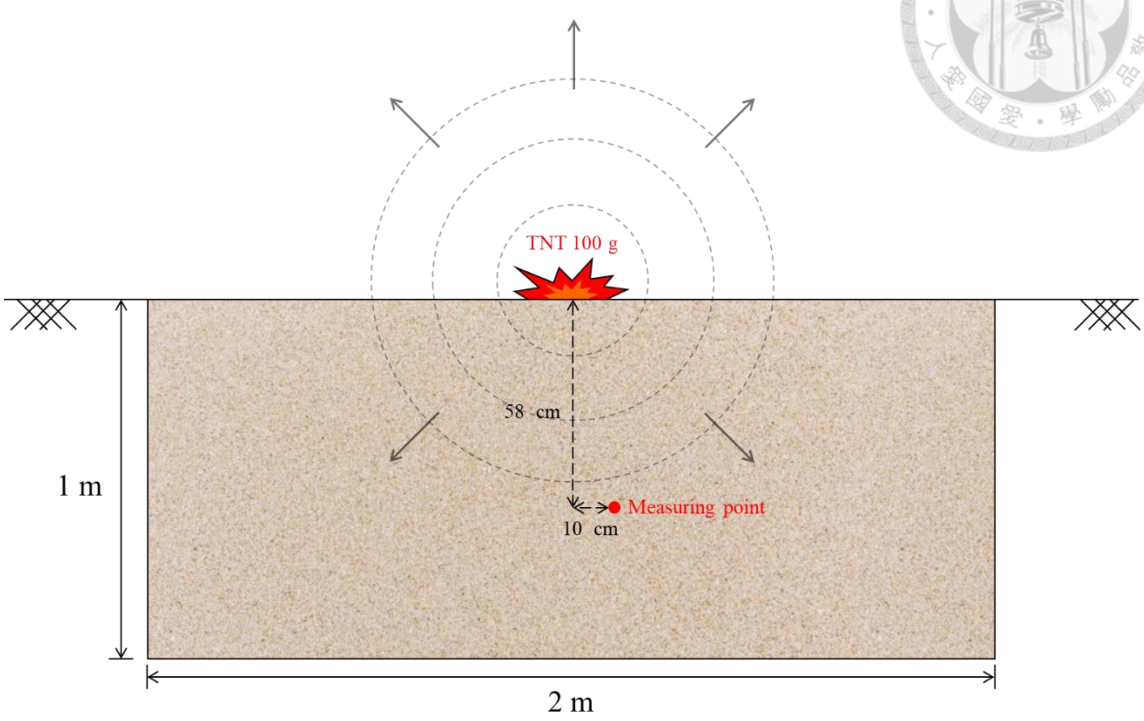

Figure 4-2 Schematic diagram for soil model validation

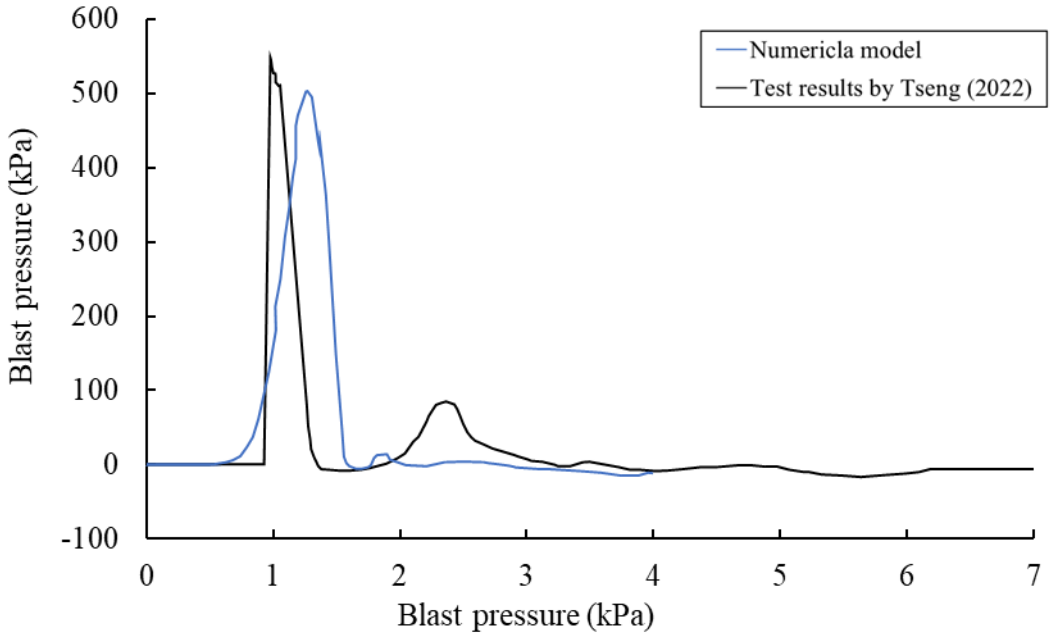

Figure 4-3 Soil pressure-time history of the numerical model and results of field experiment in Tseng et al. (2022)

doi:10.6342/NTU202401573

4.1.2. Validation of Geofoam's Numerical Model

To validate the geofoam's model parameters used in this research, reproducing of the referenced study is required. As mentioned in section 3.3.4, model parameters of geofoam's numerical model are referenced from the study conducted by Khodaparast et al. (2022). The numerical model built to replicate the aforementioned is shown in Figure 4-4. In the model, 100 kg of TNT dynamite is detonated on clayey soil. At 1.5 m below ground surface, a 1 m thick geofoam layer is added as reinforcement against blast waves. In the study of Khodaparast et al. (2022), the soil pressure is measured at 2 m and 3 m below the ground surface before the geofoam layer is added to the model. After installing geofoam, the pressure is measured at 3.5 and 4.5 m below the ground surface. Model validation in this section focuses on the peak pressure measured in the soil before and after the geofoam is added to ensure the accuracy of both soil and geofoam's modeling. Table 4-1 shows the results of geofoam model validation. By comparing the numerical results with the referenced study, it can be observed that the error in measured peak blast pressure in the soil is within an acceptable range. This indicates a successful validation of geofoam's numerical model.

doi:10.6342/NTU202401573

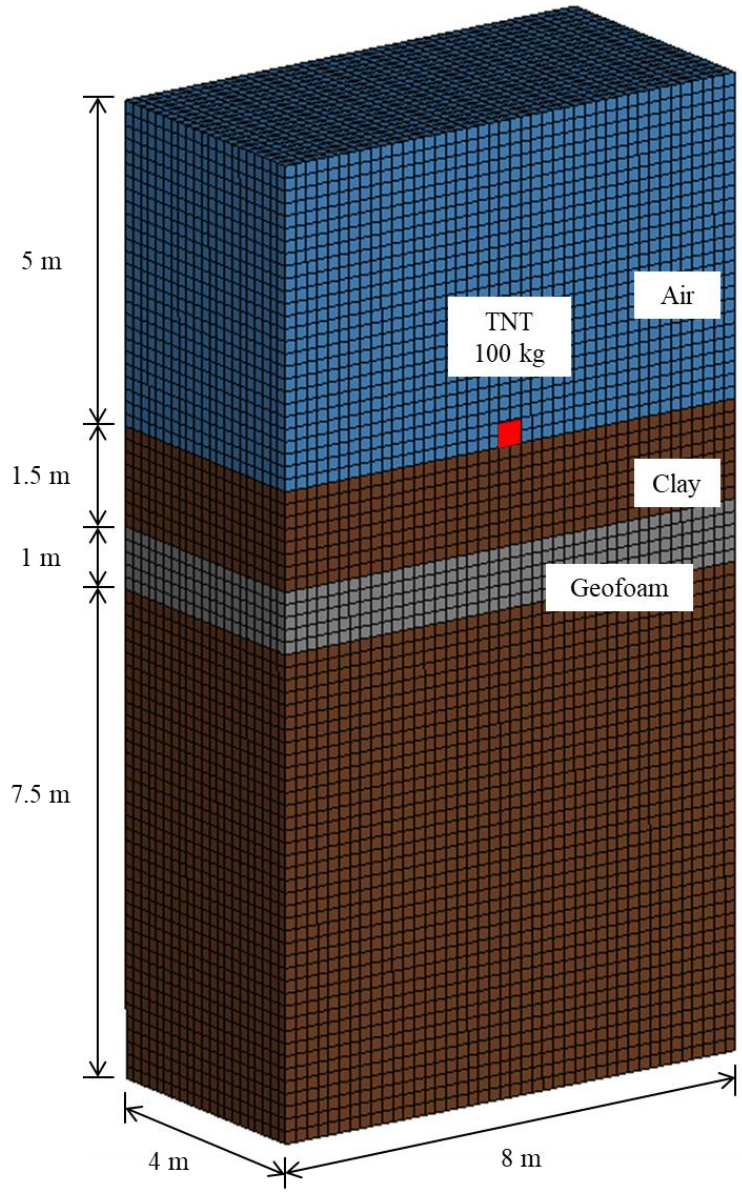

Figure 4-4 Numerical model for validation of geofoam model parameters

doi:10.6342/NTU202401573

Table 4-1 Soil peak pressure of the numerical model and results Khodaparast et al. (2022): (a) Clayey soil without geofoam. (b) Clayey soil with geofoam.

(a) Clayey soil without geofoam

Model	Peak pressure at 2 m depth (MPa)	Error (%)	Peak pressure at 3 m depth (MPa)	Error (%)
Khodaparast et al. (2022)	4.37	-	1.78	-
This study	4.23	3.21	1.76	1.12

(b) Clayey soil with geofoam

Model	Peak pressure at 3.5 m depth (MPa)	Error (%)	Peak pressure at 3.5 m depth (MPa)	Error (%)
Khodaparast et al. (2022)	0.90	-	0.67	-
This study	0.88	2.34	0.71	5.94

doi:10.6342/NTU202401573

4.2. Sensitivity Studies

The goal of the sensitivity study is to identify the most influential parameter in the numerical simulations of geofoam model validation on the blast pressure. Based on the study of Woods (1968) and Wang (2009), wave attenuation through a media is governed by its wave impedance. The wave impedance of a media is calculated through Eq.(4-1):

$$Z = \rho V = \rho\sqrt{\frac{K+\frac{4}{3}G}{\rho}} = \sqrt{\rho(K+\frac{4}{3}G)} \tag{4-1}$$

where Z is wave impedance, ρ is density, K is the bulk modulus, G is the shear modulus, and V is the speed of wave when transmitted in the material. Since this research focuses on the attenuation of soil blast pressure, the wave speed is represented by the pressure wave speed.

Eq.(4-1) indicates wave impedance is governed by three parameters: density, bulk modulus, and shear modulus. Therefore, the sensitivity study focuses on these parameters. To evaluate the effect of these parameters on the blast attenuation performance of geofoam, they are varied within a range of $\pm 50\%$.

To conduct the sensitivity study, a model is constructed as shown in Figure 4-5: a field with a depth of 5 m and a width of 10 m is constructed, and a 1-meter thick EPS 22 geofoam layer is installed 1 meter below the ground surface. To evaluate the effects of

doi:10.6342/NTU202401573

changes in geofoam on the peak blast pressure in the soil, the hydrostatic pressure of soil is measured at 3 m below ground surface where the explosive is detonated.

The results of the sensitivity study are shown in Figure 4-6 through Figure 4-8. Based on the numerical results, it can be observed that when geofoam's density varies between 0.106 and 0.318 kN/m^3 ($0.216\text{kN/m}^3 \pm 50\%$), the difference in peak blast pressure reaches up to 0.4 MPa. In comparison, when the geofoam's bulk modulus varies between 1.115 and 3.345 MPa ($2.23\text{MPa} \pm 50\%$), the difference in peak blast pressure is 0.079 MPa. Similarly, when the geofoam's shear modulus varies between 1.125 and 3.375 MPa ($2.25\text{MPa} \pm 50\%$), the difference in peak blast is 0.022 MPa. The results of the sensitivity study indicate that the geofoam's density is the most influential parameter among geofoam's properties.

doi:10.6342/NTU202401573

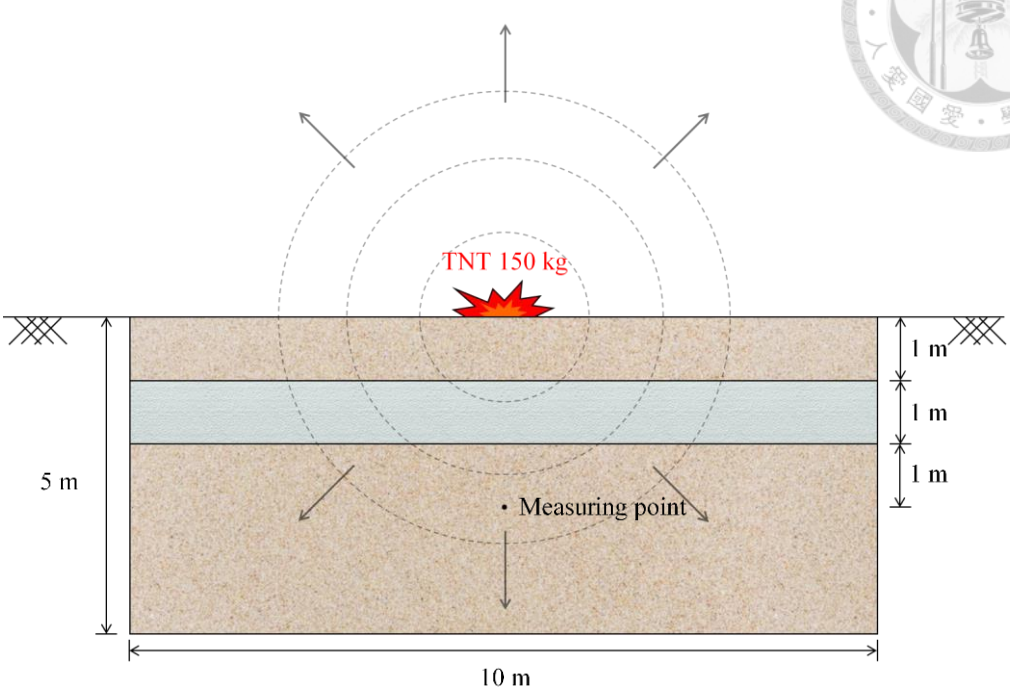

Figure 4-5 Schematic diagram for sensitivity study

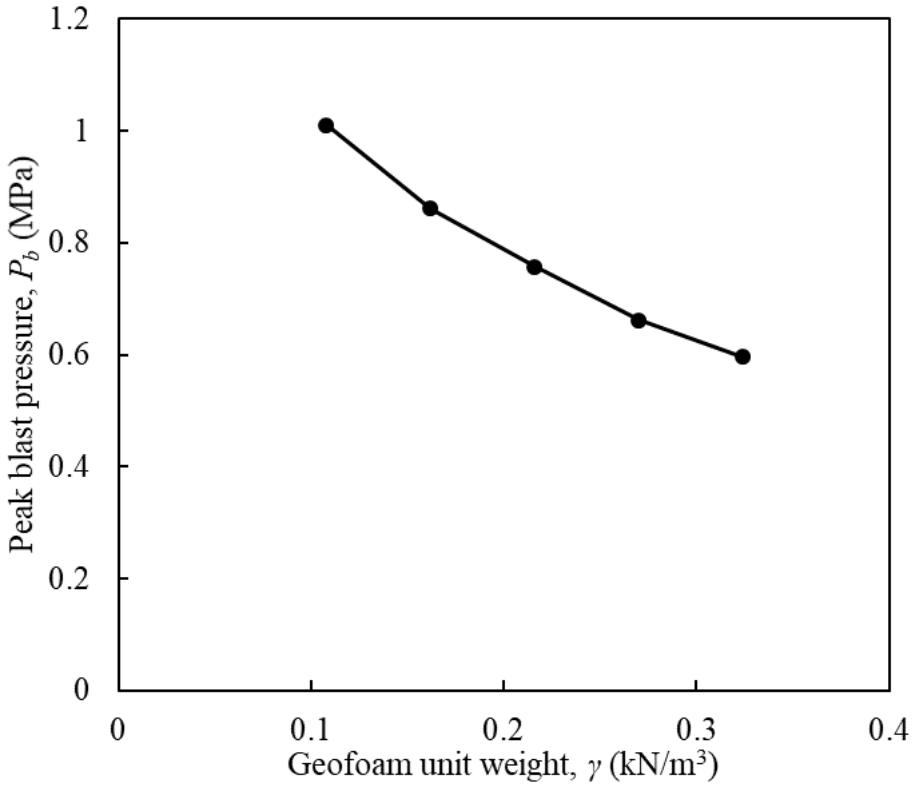

Figure 4-6 Geofoam unit weight's effect on peak blast pressure

doi:10.6342/NTU202401573

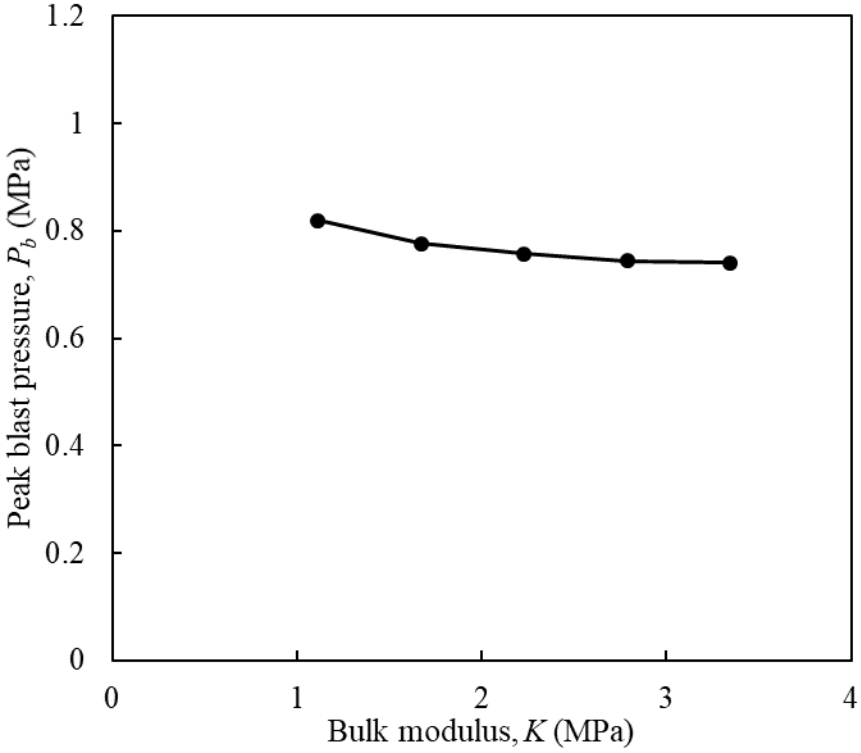

Figure 4-7 Geofoam bulk modulus' effect on peak blast pressure

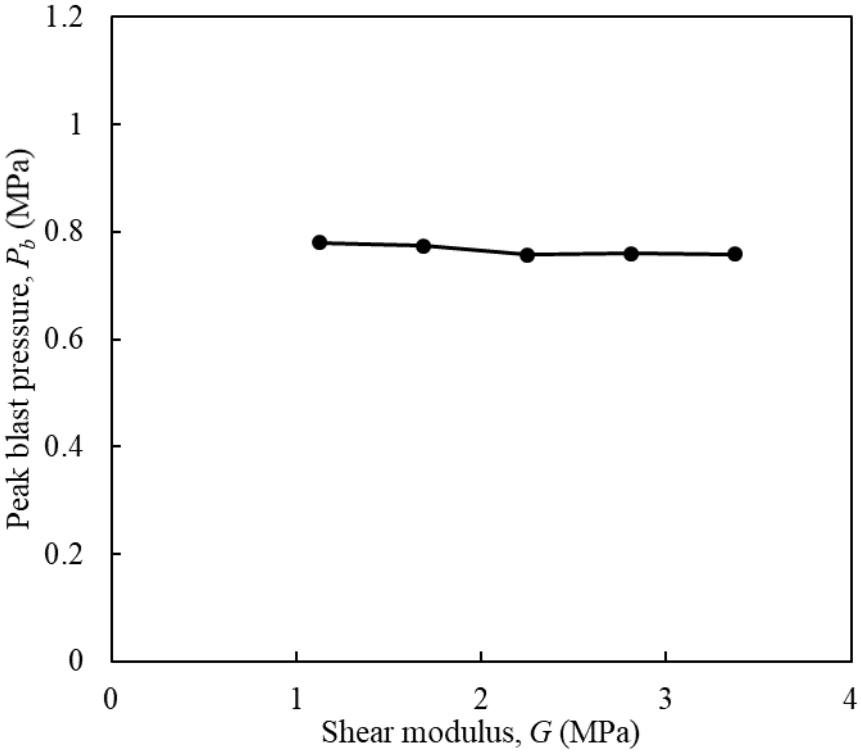

Figure 4-8 Geofoam shear modulus' effect on peak blast pressure

doi:10.6342/NTU202401573

Chapter 5. Results and Discussions

In this chapter, the behavior of soil under blast load is discussed. The results and discussions are presented in four sections:

1. An introduction to the response of unreinforced ground under the influence of 150 kg of TNT detonating on the ground surface.

2. Discussions and comparisons of the dynamic behavior of soil with and without geofoam reinforcements.

3. Parametric studies to investigate the best layout for the geofoam-reinforced blast attenuation layer.

4. Based on the aforementioned results, a recommended layout for the blast attenuation layer is proposed.

5.1. Response of Unreinforced Ground Subjected to Blast Load

Figure 3-3 and Figure 3-4 illustrate the numerical model and schematic diagram for the full-scale model of explosives denotated on unreinforced ground surface. Figure 5-1 ~ Figure 5-4 shows the numerical results. To ensure the credibility of the full-scale unreinforced ground model, the obtained results are first compared with the prediction

doi:10.6342/NTU202401573

made by the U.S. Army manual TM 5-855-1. Four soil models from the TM 5-855-1 manual representing the sandy soil were selected for comparison. Figure 5-1 illustrates the peak blast pressure at different depths predicted by empirical equations and the numerical model. It can be noticed that the prediction made by the numerical model closely matches the estimations of the empirical equations.

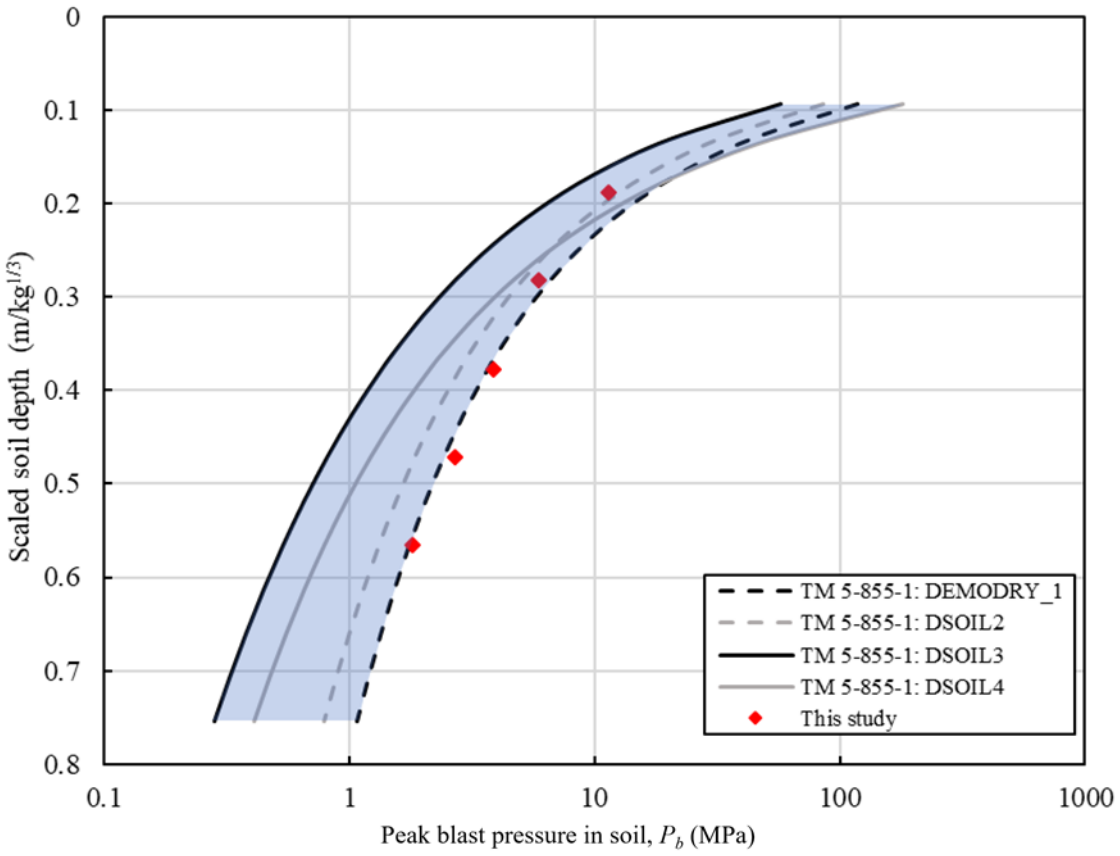

Figure 5-1 Comparison of unreinforced ground's numerical results and predictions of TM 5-855-1

doi:10.6342/NTU202401573

Figure 5-1 shows that the numerical model aligns closely with the prediction made by the soil model DEMODRY_1. Figure 5-2 illustrates the comparison between the predictions of the numerical model and the DEMODRY_1 mode. The blue area outlines the ±10% range of the empirical equation's estimation. It was found that the numerical model falls within the region compared to the empirical equation. This high degree of similarity could be due to the fact that both the numerical model and DEMODRY_1 model share similar properties in terms of density, specific gravity, and water content. Such similarities could lead to comparable dynamic behaviors under the influence of blast loads.

doi:10.6342/NTU202401573

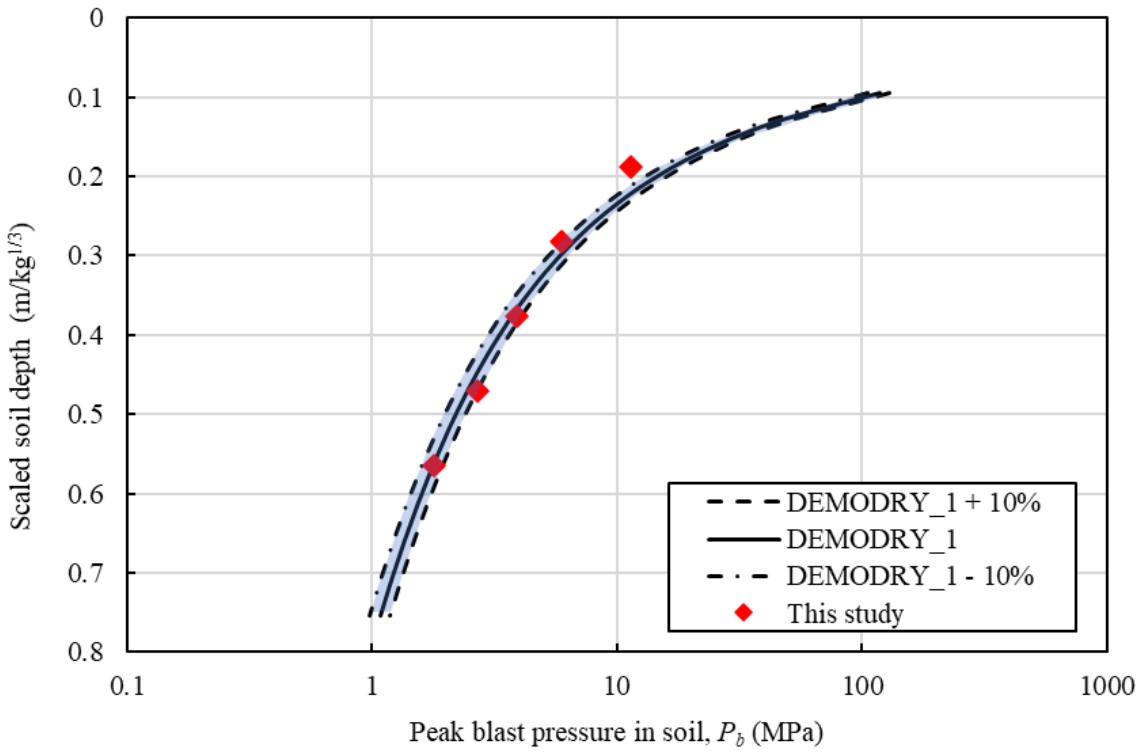

Figure 5-2 Comparison of unreinforced ground's numerical results and DEMODRY_1 soil model

Based on the time history shown in Figure 5-3, it can be noticed that blast pressure in soil 3 m below the surface reached its peak at 17.5 ms, with a peak blast pressure reading of 1.93 MPa. The duration of the shock wave lasted for 4 ms, and once the shock front passed through, the pressure buildup in soil dissipated rapidly. Figure 5-4 shows the time history of vertical acceleration recorded in soil 3 m below the ground surface. The recorded vertical acceleration reached its peak at 16.5 ms, with a reading of 723.751g. It is observed that the time of arrival for blast pressure has a 1 ms delay compared to that of vertical acceleration.

doi:10.6342/NTU202401573

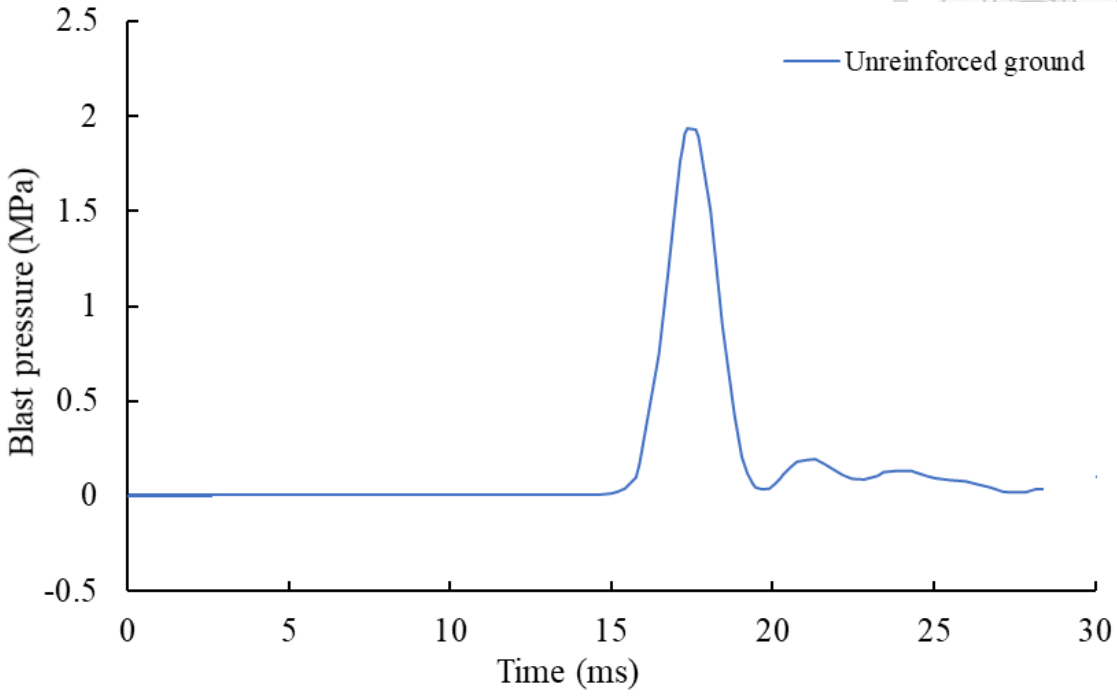

Figure 5-3 Time history of blast pressure in unreinforced ground

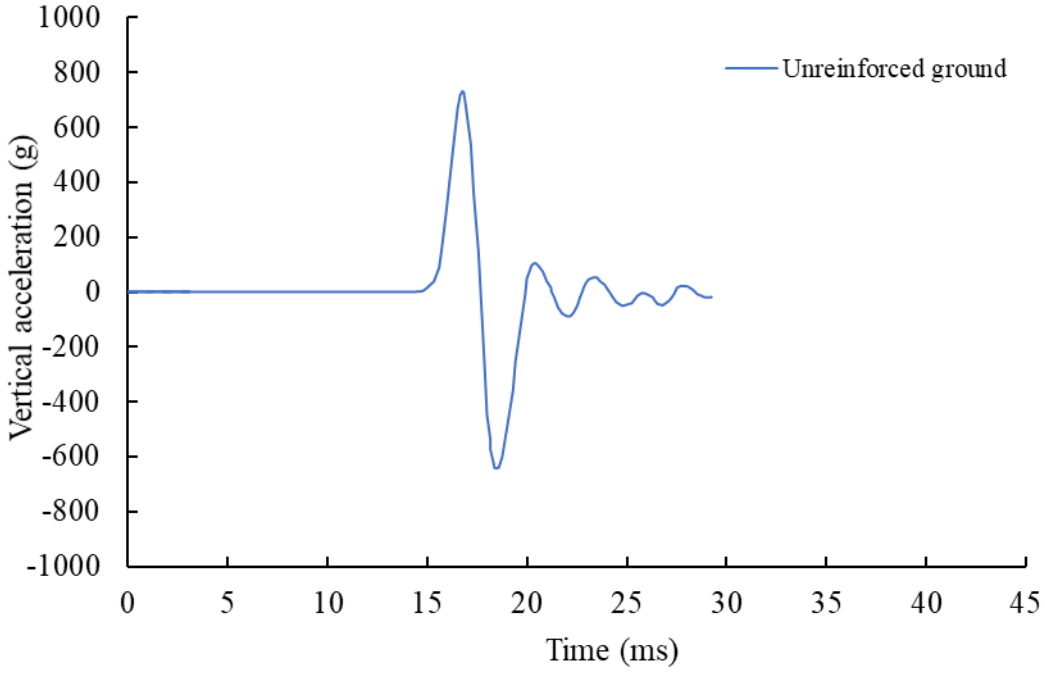

Figure 5-4 Time history of vertical acceleration in unreinforced ground

doi:10.6342/NTU202401573

5.2. Response of Geofoam-Reinforced Ground Subjected to Blast Load

Figure 3-5 and Figure 3-6 illustrate the numerical model outline and its schematic diagram for the geofoam-reinforced ground model. As shown in both figures, a 1-meter thick EPS 22 geofoam layer is installed 1 m below the ground surface as reinforcement against blast waves.

Figure 5-5 shows the comparison of shock wave propagation between the reinforced ground model and the unreinforced ground model. After the explosive's detonation, the transmission of two shock fronts in the soil can be observed: one is the shock wave directly transmitted from the explosion to the soil, and the other is the shock wave first transmitted from the blast to the air then into the soil. At t = 0.1 to 6 ms, little difference between the two models can be noticed. However, as the shock front reaches the geofoam layer, as shown in Figure 5-6 d , the shock front rapidly dissipates through the geofoam. In comparison, the pressure contour for the unreinforced ground model maintained a relatively intact shock front with a higher blast pressure value. By the end of the simulation process, the shock wave in the reinforced ground model had almost been absorbed by the geofoam, indicating the shock wave was effectively dissipated.

doi:10.6342/NTU202401573

During the wave transmission process, it can be observed that the shock traveled more rapidly in geofoam compared to soil. The pressure wave velocity is estimated through Eq.(5-1)

$$V_P = \sqrt{\frac{K + \frac{4}{3}G}{\rho}} \tag{5-1}$$

where V_p is pressure wave velocity, ρ is density, K is the bulk modulus, and G is the shear modulus. Table 5-1 shows the pressure wave velocity of the quartz sand and geofoam. It can be noticed that the pressure wave transmits faster in geofoams than in soil. This observation is compliant with the numerical results.

Based on the study of Wang (2009), the shock wave attenuation effect of geofoam is achieved through the difference in wave impedance between soil and geofoam. The wave impedance of quartz sand and geofoam are listed in Table 5-1. Since the wave impedance of quartz sand is larger than that of geofoams by at least an order, energy transmission between soil and geofoam is inefficient, which is compliant with the numerical results.

doi:10.6342/NTU202401573

Table 5-1 Wave impedance of quartz sand and geofoams

Material	Density, ρ (kg/m^3)	Pressure wave velocity, V_P (m/s)	Wave impedance, Z (kg/m^{2}s)
Quartz sand	1604	149.17	2.39E+05
EPS 15 geofoam	14.42	414.151	5.97E+03
EPS 22 geofoam	21.62	491.783	1.06E+04
EPS 39 geofoam	38.44	568.572	2.19E+04

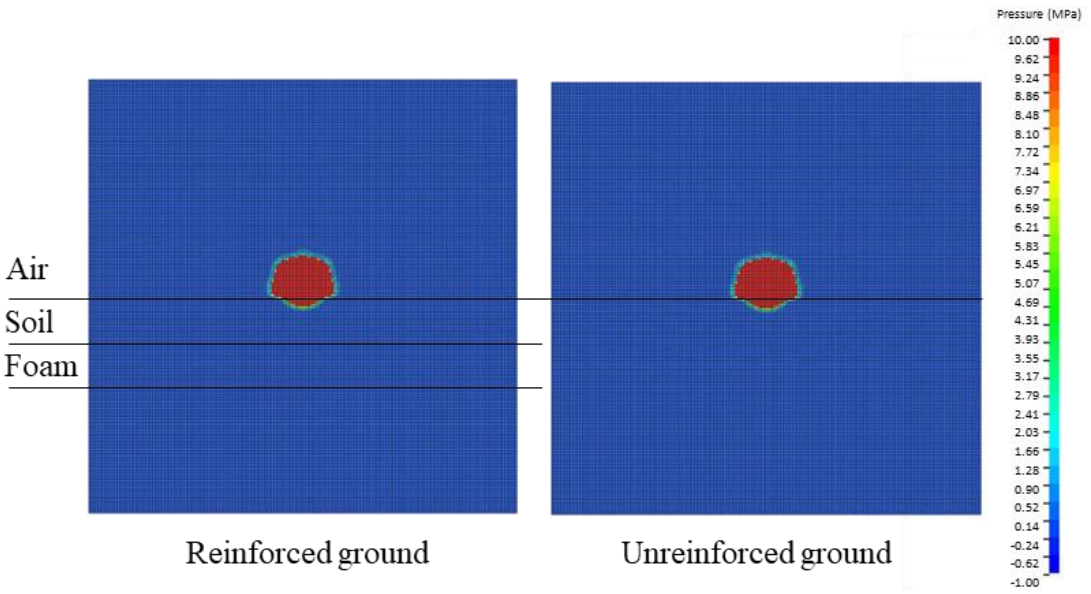

(a) t = 0.1 ms

doi:10.6342/NTU202401573

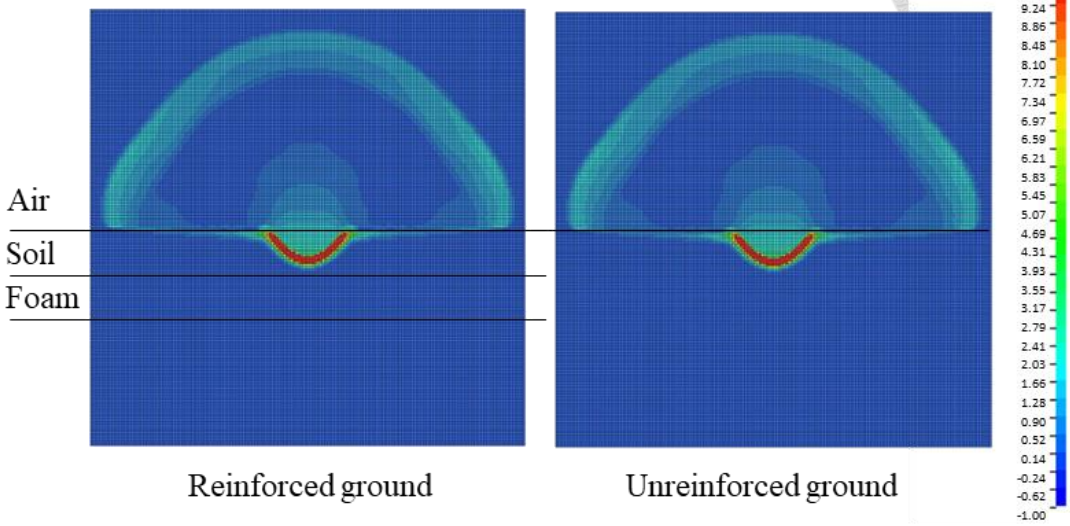

(b) t = 2 ms

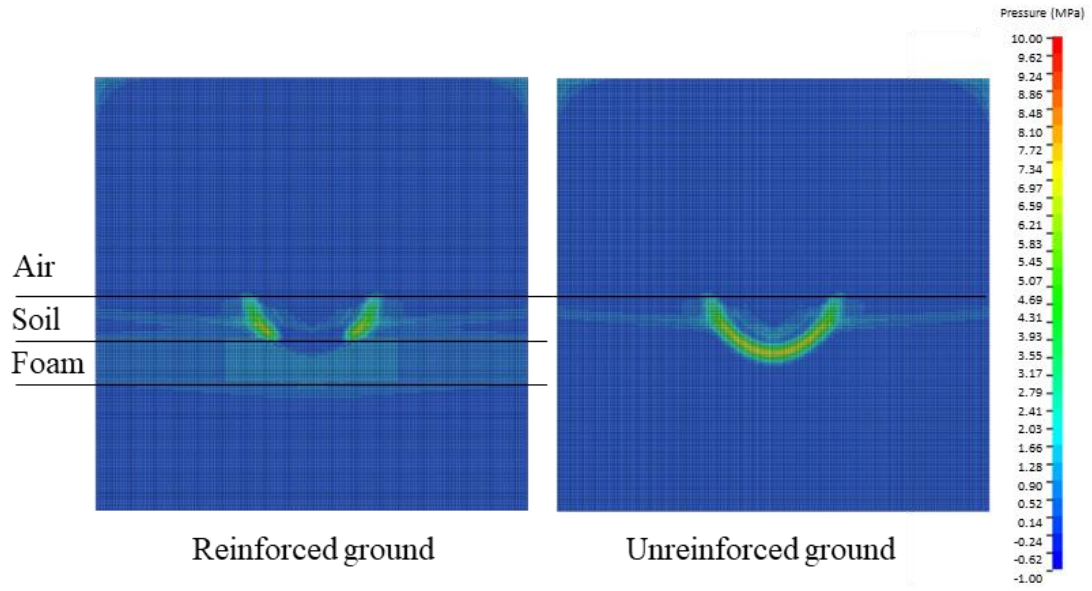

(c) t = 6 ms

doi:10.6342/NTU202401573

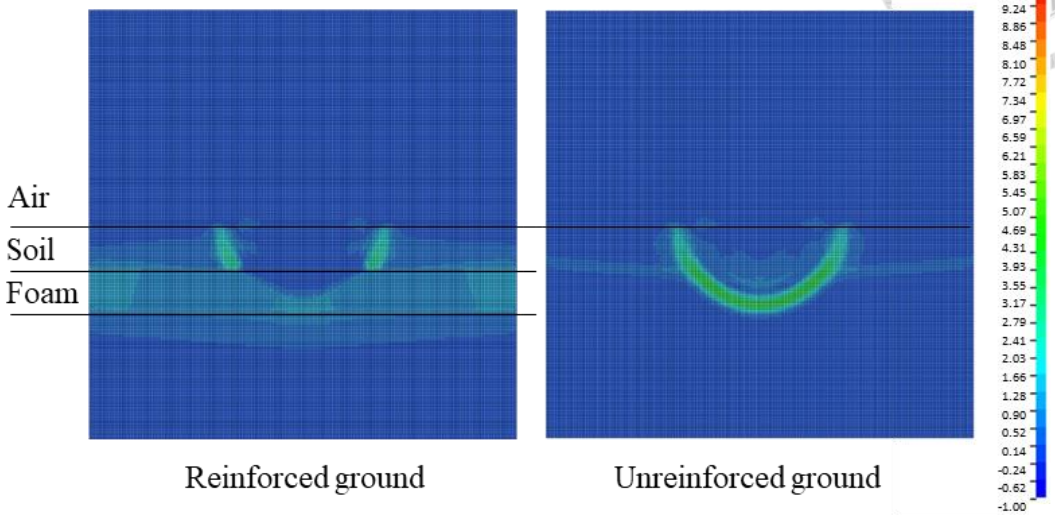

(d) t = 10 ms

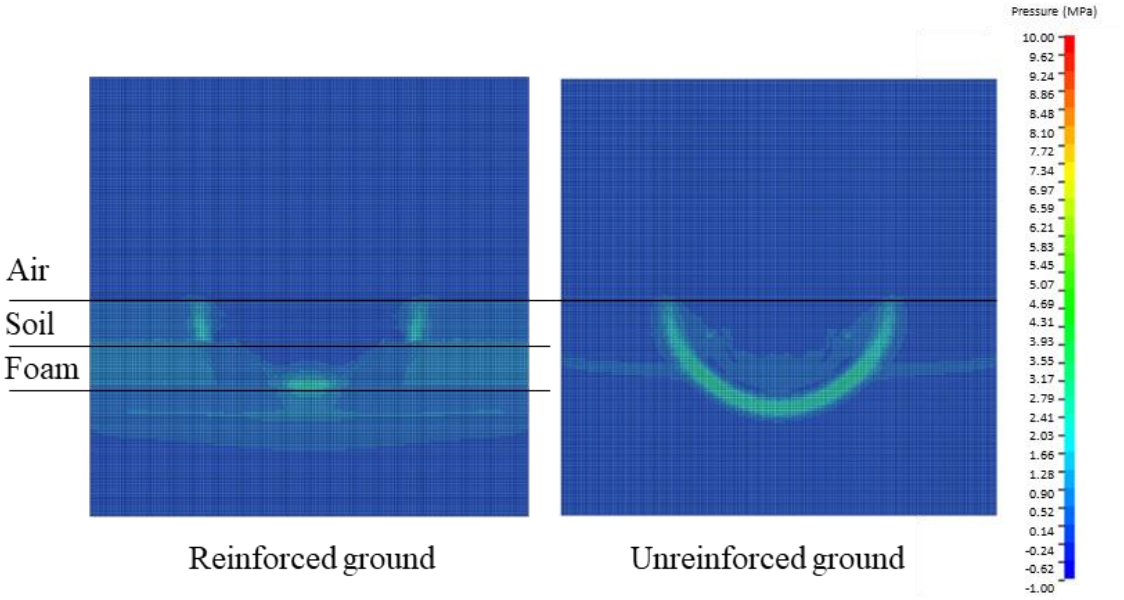

(e) t = 15 ms

doi:10.6342/NTU202401573

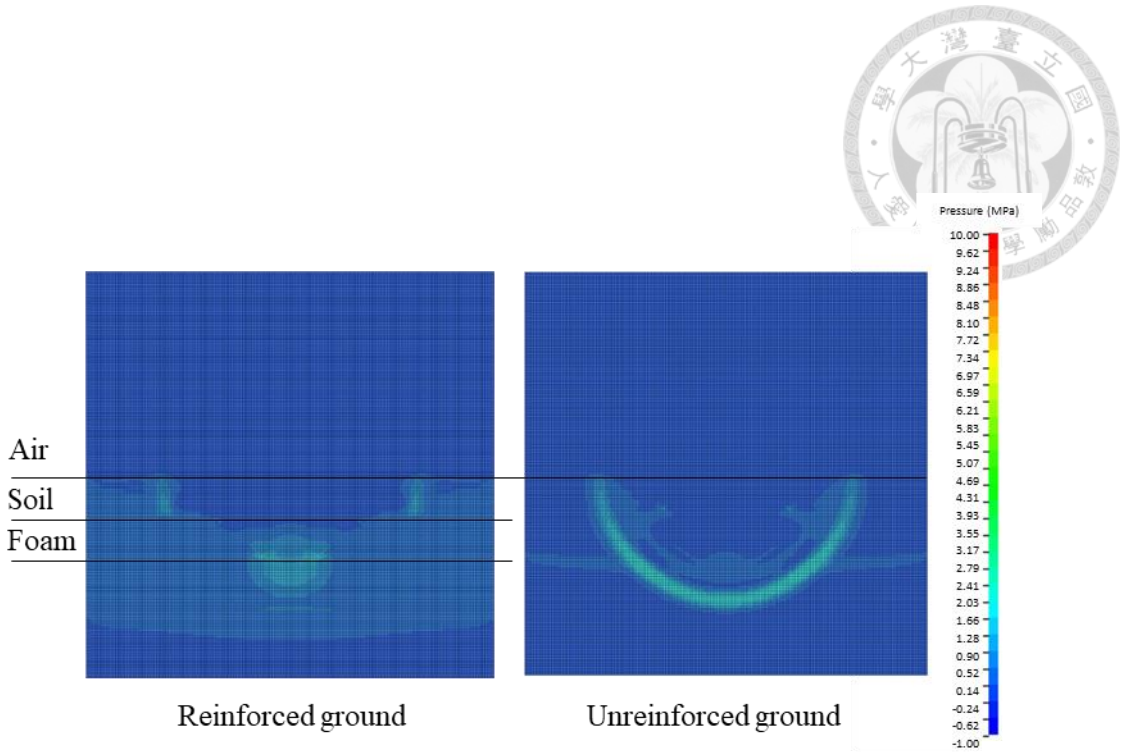

(f) t = 20 ms

Figure 5-5 Comparison of shock wave propagation in the reinforced ground and unreinforced ground, t = (a) 0.1 ms; (b) 2 ms; (c) 6 ms; (d) 10 ms; (e) 15 ms; (f) 20 ms

To evaluate the reduction in peak blast pressure and peak vertical acceleration in soil, a parameter called “Reduction factor” is developed. The reduction factor is obtained through Eq.(5-2) and Eq.(5-3)

$$RD_b = \frac{P_{b_{sand}} - P_{b_{reinforced}}}{P_{b_{sand}}} \times 100\% \quad (5\text{-}2)$$

doi:10.6342/NTU202401573

where RD_b is the reduction factor in peak blast pressure, $P_{b_{sand}}$ is the peak blast pressure measured in the unreinforced ground model, whereas $P_{b_{reinforced}}$ represents the peak blast pressure measured in the geofoam-reinforced ground model.

$$RD_a = \frac{a_{v_{sand}} - a_{v_{reinforced}}}{a_{v_{sand}}} \times 100\% \tag{5-3}$$

where RD_a is the reduction factor in peak vertical acceleration $a_{v_{sand}}$ is the peak vertical acceleration measured in the unreinforced ground model, whereas $a_{v_{reinforced}}$ represents the peak vertical acceleration measured in the geofoam-reinforced ground model.

The shock wave attenuation performance of geofoam reinforced ground in terms of P_b and a_v are shown in Table 5-2. Comparing the time history of blast pressure in Figure 5-6, after geofoam reinforcement is installed, P_b is reduced by 60.77% from 1.930 MPa to 0.384 MPa. Apart from the reduction in P_b , it is also observed that the time of arrival for P_b is delayed by 5 ms. In terms of the duration of the shock wave, after geofoam reinforcement, the duration of shock wave was prolonged from 5 ms to over 30 ms. Through geofoam reinforcement, the shock wave's energy release is transformed from a short duration with high-pressure readings to a longer duration with significantly lower pressure readings.

doi:10.6342/NTU202401573

Table 5-2 Comparison of P_b and a_v in unreinforced and reinforced ground

Model	Peak blast pressure P_b (MPa)	Peak vertical acceleration a_v (g)
Unreinforced ground	1.930	723.751
Reinforced ground	0.384	121.329
Reduction ratio, *RD* (%)	60.77	83.24

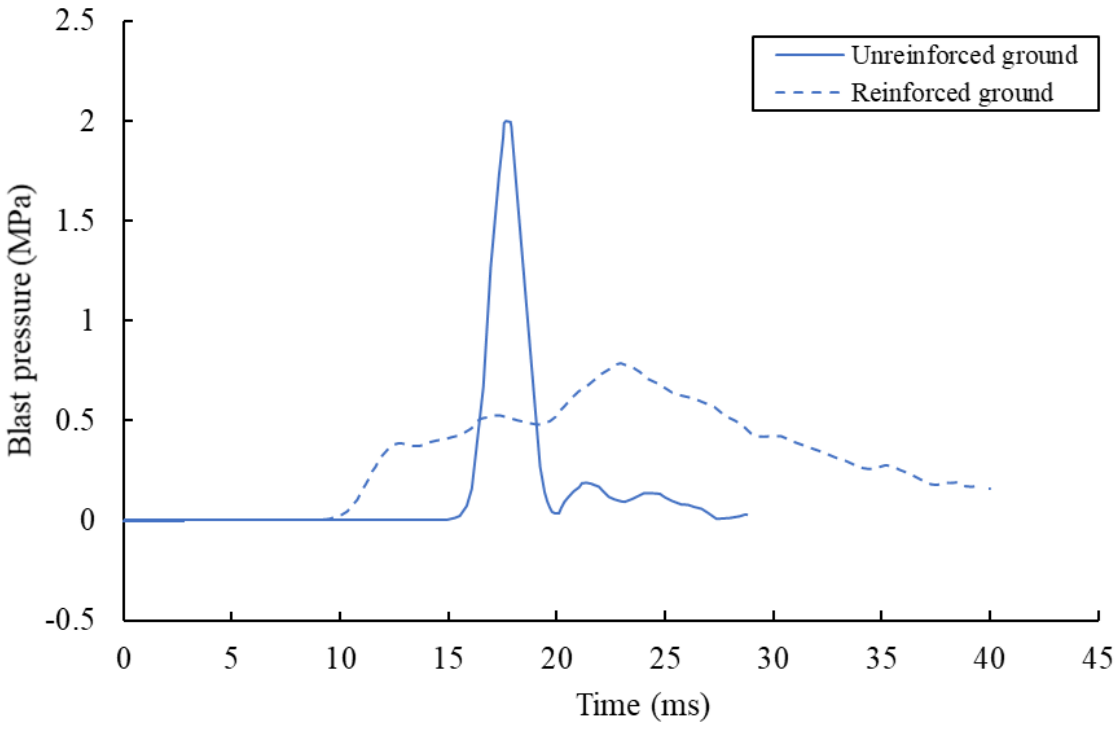

Figure 5-6 Time history of blast pressure in soil

doi:10.6342/NTU202401573

The numerical results for the vertical acceleration of soil particles are shown in Figure 5-7. After geofoam reinforcement, the peak vertical acceleration (a_v) of the soil particles decreased from 723.751g to 121.329g, representing an 83.24% reduction in a_v.

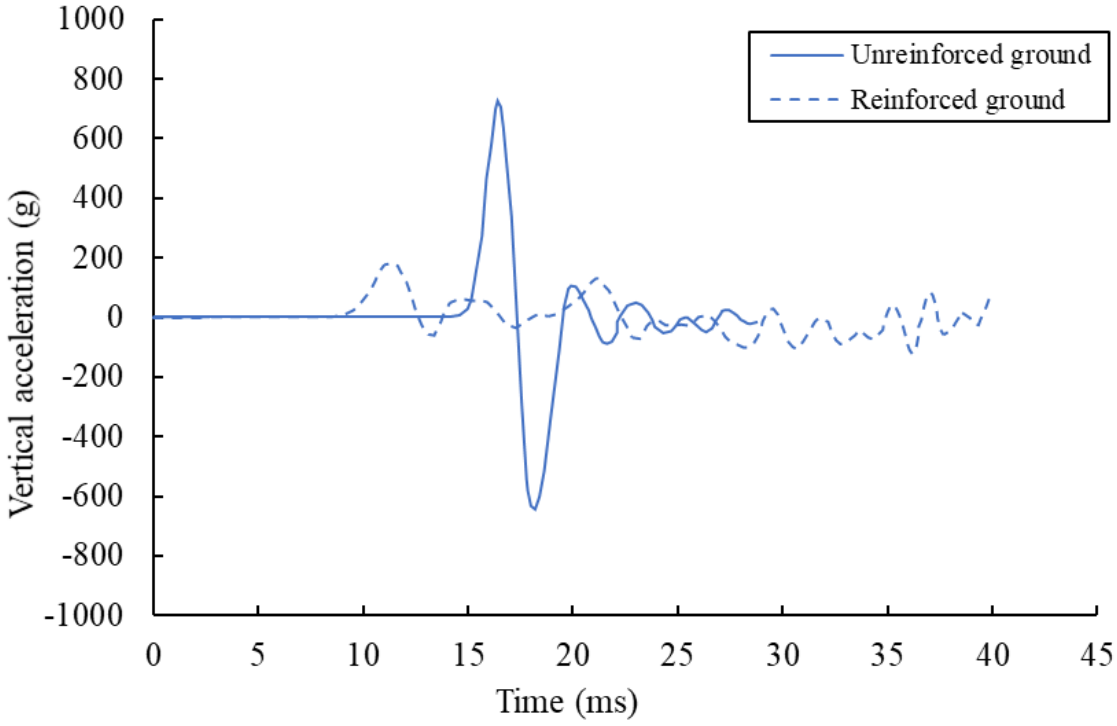

Figure 5-7 Time history of vertical acceleration in soil

doi:10.6342/NTU202401573

5.3. Parametric Studies

In this section, parametric studies were conducted to evaluate the most efficient layout for a geofoam-reinforced shock wave attenuation layer. The numerical study program is listed in Table 5-3. The parametric study focuses on three properties of the geofoam reinforcement: the type of geofoam used, the thickness of geofoam reinforcement, and the embedded depth of geofoam reinforcements. The effects of these parameters on P_b and a_v are investigated. In this research, the coverage of geofoam's effect on shock wave attenuation performance is not considered. It is assumed that the geofoam fully covers the underground shelter to prevent potential diffractions of shock waves.

doi:10.6342/NTU202401573

Table 5-3 Numerical study program

Parameter	EPS type	Density γ (kN/m^3)	Bulk modulus K (MPa)	Shear modulus G (MPa)	Geofoam thickness t (m)	Geofoam embedded depth D (m)
Unreinforced	-	-	-	-	-	-
Baseline case	EPS 22	0.212	2.23	2.25	1	1
Geofoam type	EPS 39	0.384	4.24	6.14	1	1
	EPS 15	0.144	1.14	1	1	1
Geofoam thickness	EPS 22	0.212	2.23	2.25	1.5	1
	EPS 22	0.212	2.23	2.25	1.25	1
	EPS 22	0.212	2.23	2.25	0.75	1
	EPS 22	0.212	2.23	2.25	0.5	1
Embedded depth	EPS 22	0.212	2.23	2.25	1	1.5
	EPS 22	0.212	2.23	2.25	1	1.25
	EPS 22	0.212	2.23	2.25	1	0.75
	EPS 22	0.212	2.23	2.25	1	0.5

5.3.1. Geofoam Type

To investigate the effect of geofoam type on shock wave attenuation, three types of geofoams are selected based on the ATSM D6817 standards: EPS 15, EPS 22, and EPS 39. Based on the sensitivity studies conducted in Chapter 3, geofoam density is the most influential factor in geofoam's shock wave attenuation performances. Thus, in the parametric study, the differences in geofoam type are considered with respect to their densities.

The results of the parametric study on geofoam type are presented in Figure 5-8. The figure indicates that as the geofoam's density increases, the peak blast pressure and peal vertical acceleration also increase. Such observation suggests that the geofoam's density is positively related to its shock wave attenuation performance. This claim is supported by differences in geofoam's wave impedance: as shown in Table 5-1, geofoam's density is positively related to its wave impedance. A higher wave impedance leads to a higher energy dissipation as shock waves pass through.

Based on the numerical results listed in Table 5-4 and Table 5-5, a shock wave attenuation layer installed with EPS 39 geofoam would result in a 70.6% reduction in P_b

doi:10.6342/NTU202401573

and 87.17% reduction in a_v. In comparison, when EPS 15 geofoam is used, RD_b and RD_a are reduced to 49.22% and 73.5 %, respectively.

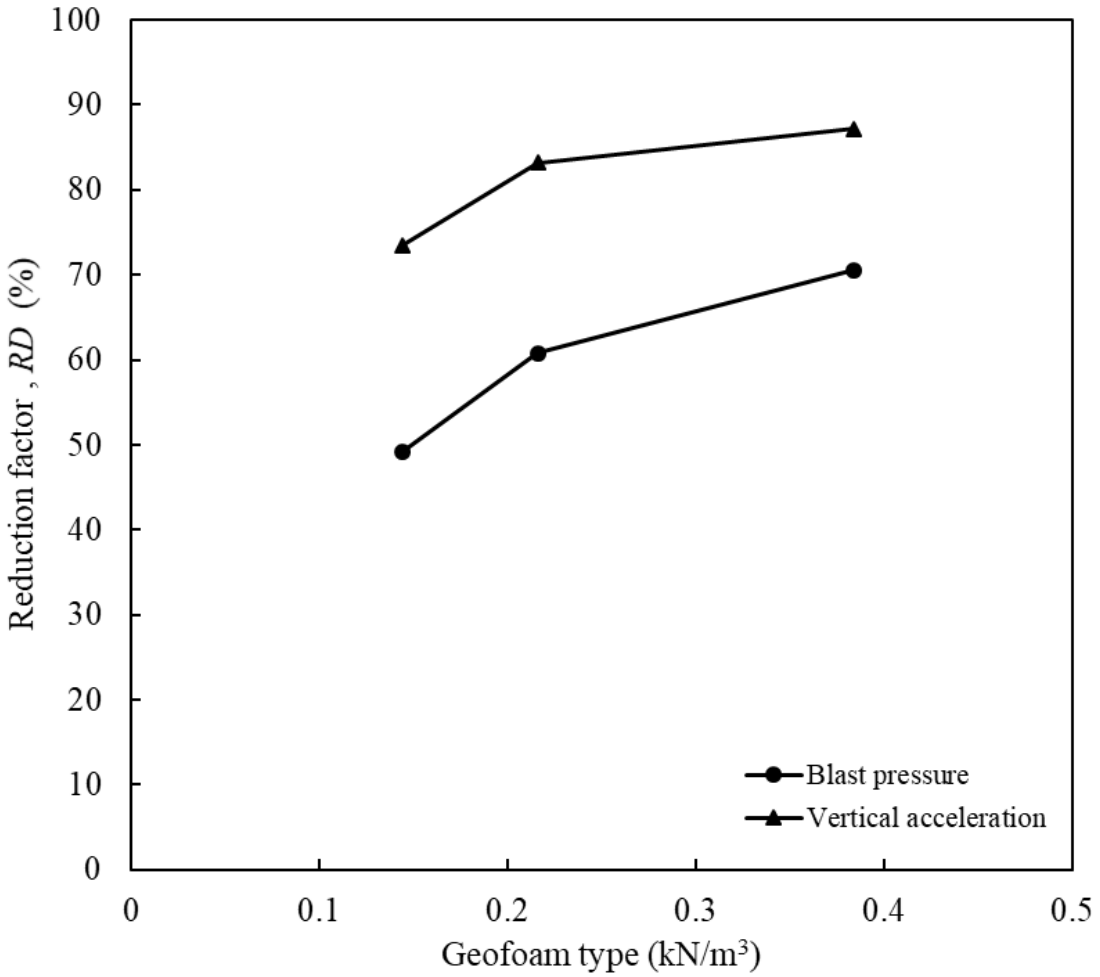

Figure 5-8 Geofoam type's effect on reduction factor

doi:10.6342/NTU202401573

Table 5-4 Numerical study results: reduction in peak blast pressure

Parameter	EPS type	Geofoam thickness, t (m)	Geofoam embedded depth, D (m)	Peak blast pressure, P_b (MPa)	Reduction factor, RD_b (%)
Unreinforced ground	-	-	-	1.930	-
Baseline case	EPS 22	1	1	0.757	60.77
Geofoam type	**EPS 15**	1	1	0.980	49.22
	EPS 39	1	1	0.567	70.60
Geofoam thickness	EPS 22	**0.50**	1	1.311	32.09
	EPS 22	**0.75**	1	1.073	44.39
	EPS 22	**1.25**	1	0.602	68.81
	EPS 22	**1.50**	1	0.470	75.64
Embedded depth	EPS 22	1	**0.50**	2.011	-4.21
	EPS 22	1	**0.75**	1.483	23.15
	EPS 22	1	**1.25**	0.465	75.91
	EPS 22	1	**1.50**	0.402	79.16

Table 5-5 Numerical study results: reduction in peak vertical acceleration

Parameter	EPS type	Geofoam thickness, t (m)	Geofoam embedded depth, D (m)	Peak vertical acceleration, a_v (g)	Reduction factor, RD_a (%)
Unreinforced ground	-	-	-	723.751	-
Baseline case	EPS 22	1	1	121.329	83.24
Geofoam type	**EPS 15**	1	1	191.762	73.50
	EPS 39	1	1	92.836	87.17
Geofoam thickness	EPS 22	**0.50**	1	68.873	68.87
	EPS 22	**0.75**	1	71.408	71.41
	EPS 22	**1.25**	1	93.176	93.18
	EPS 22	**1.50**	1	89.849	89.85
Embedded depth	EPS 22	1	**0.50**	680.938	5.92
	EPS 22	1	**0.75**	289.501	60.00
	EPS 22	1	**1.25**	74.516	89.70
	EPS 22	1	**1.50**	32.620	95.49

doi:10.6342/NTU202401573

5.3.2. Thickness of Geofoam

In this section, the effect of geofoam's thickness (*t*) on shock wave attenuation is discussed. For the baseline case, a thickness of 1 meter is determined according to the standard manufacturing specifications of geofoams. In the parametric study, geofoam thickness ranging from 0.5 m to 1.5 m are considered. The other specifications for the numerical models are listed in Table 5-3.

The results of parametric study on geofoam type are presented in Figure 5-9. The figure indicates that parameter *t* is positively related to the shock wave attenuation layer's performance: $t = 1.5\text{m}$, $RD_b = 75.64\%$, $RD_a = 89.85\%$. Comparatively, once $t = 0.5\text{m}$, $RD_b = 32.09\%$ and $RD_a = 68.87\%$, respectively. Based on the parametric study conducted on geofoam's thickness's effect on shock wave attenuation, a thickness of 1.5 meter is recommended.

doi:10.6342/NTU202401573

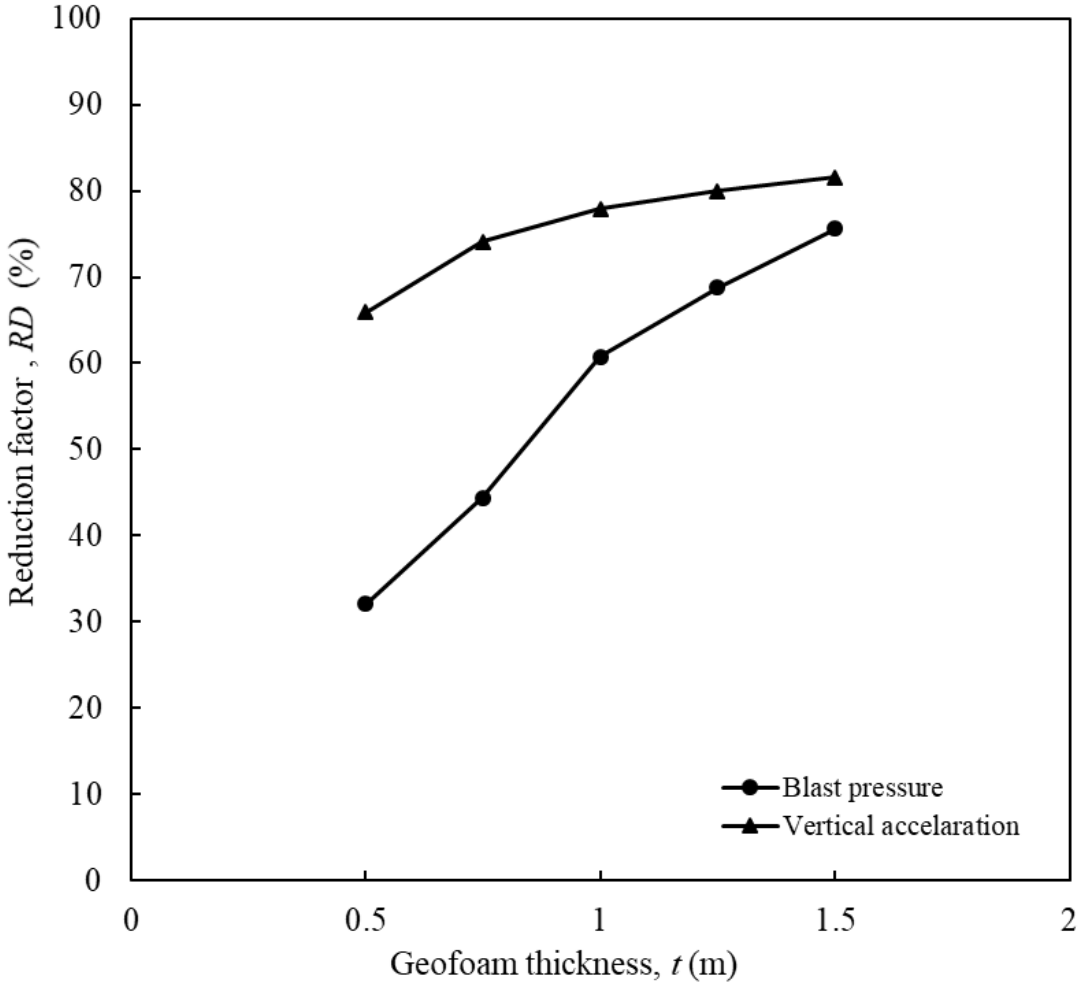

Figure 5-9 Geofoam thickness' effect on reduction factor

doi:10.6342/NTU202401573

5.3.3. Embedded Depth of Geofoam

In this section, the effect of geofoam's embedded depth (*D*) on shock wave attenuation is discussed. For the baseline case, a depth of 1 meter is determined. In the parametric study, similar to the previous section, parameter *D* ranges from 0.5 m to 1.5 m, with an interval of 0.25 m. The other specifications for the numerical models are listed in Table 5-3.

The results of parametric study on geofoam depth are presented in Figure 5-10. Comparing the effect of *D* on shock wave attenuation to other parameters, it can be observed that *D* has a significant influence on both P_b and a_v: as *D* increases, the reduction factor for P_b and a_v increases. When $D = 0.5$ m, $RD_b = -4.21\%$. Indicating that this model's performance is worse than the unreinforced ground model.

Figure 5-10 compares the shockwave's propagation between unreinforced ground and reinforced ground with 0.5 m backfill soil. The results indicate that when $t = 6$ ms, the shock front breaks through the geofoam layer and keeps propagating through the soil layer beneath the geofoam, similar to the unreinforced ground. This indicates that the geofoam layer loses its protective function as shock wave attenuation material.

doi:10.6342/NTU202401573

This result implies that for geofoam to fully perform its potential in shock wave attenuation, it requires sufficient confining pressure for geofoams to develop sufficient compressive strength to resist blast loads. Once the backfill thickness exceeds 0.5 m, the reduction factor in both P_b and a_v rapidly exceeds 60%. With a backfill thickness of 1.5 m, the reduction factors for P_b and a_v are 79.16 % and 95.49 %, respectively.

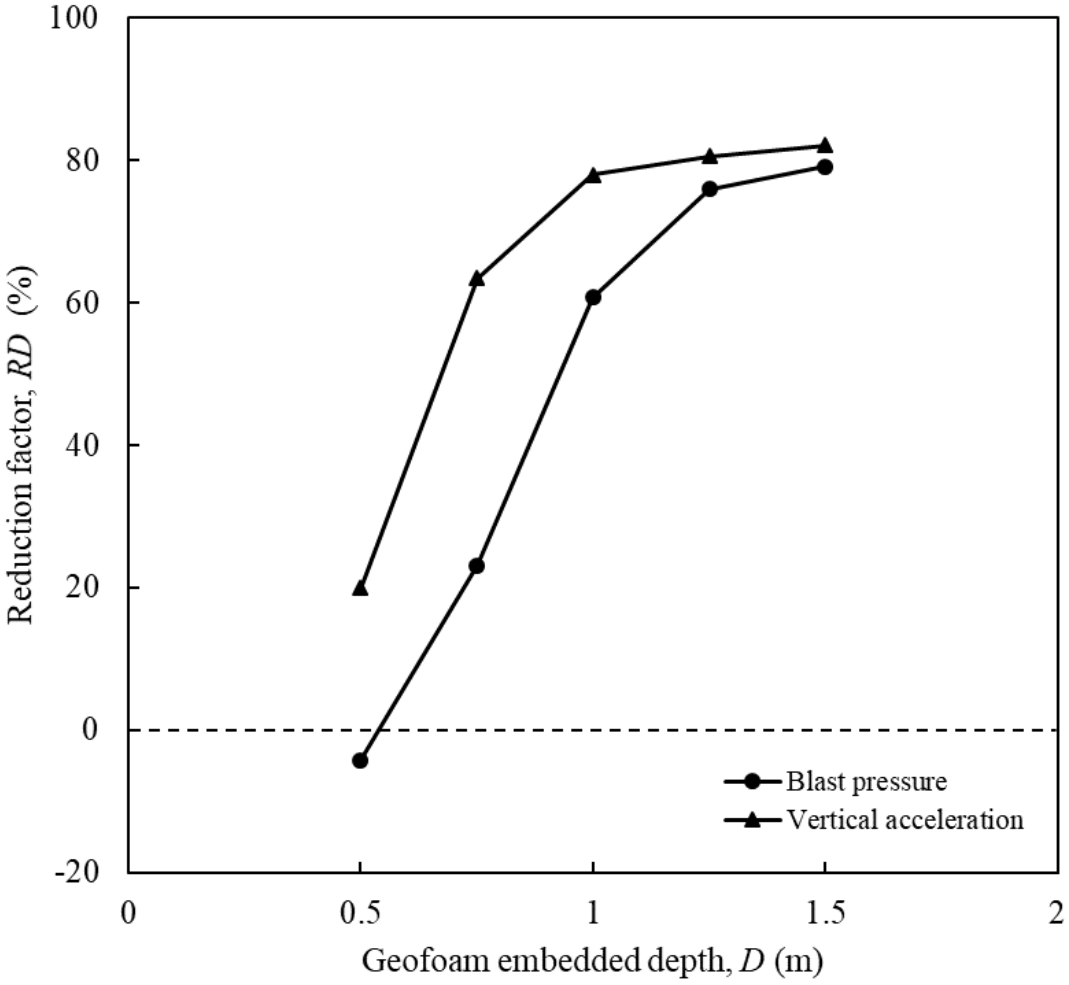

Figure 5-10 Geofoam embedded depth's effect on reduction factor

doi:10.6342/NTU202401573

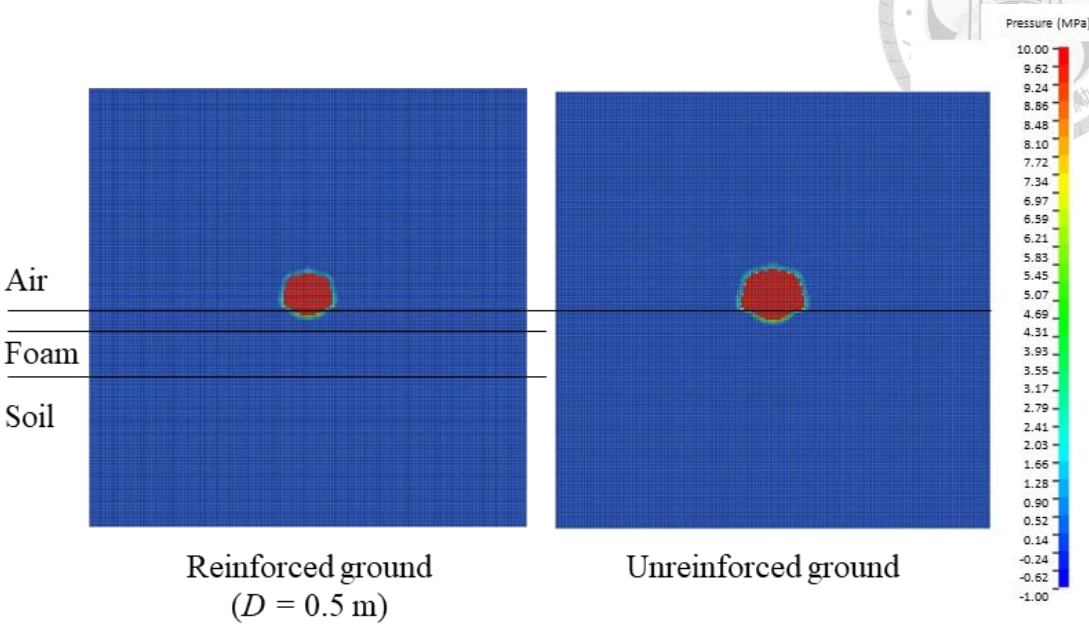

(a) t = 0.1 ms

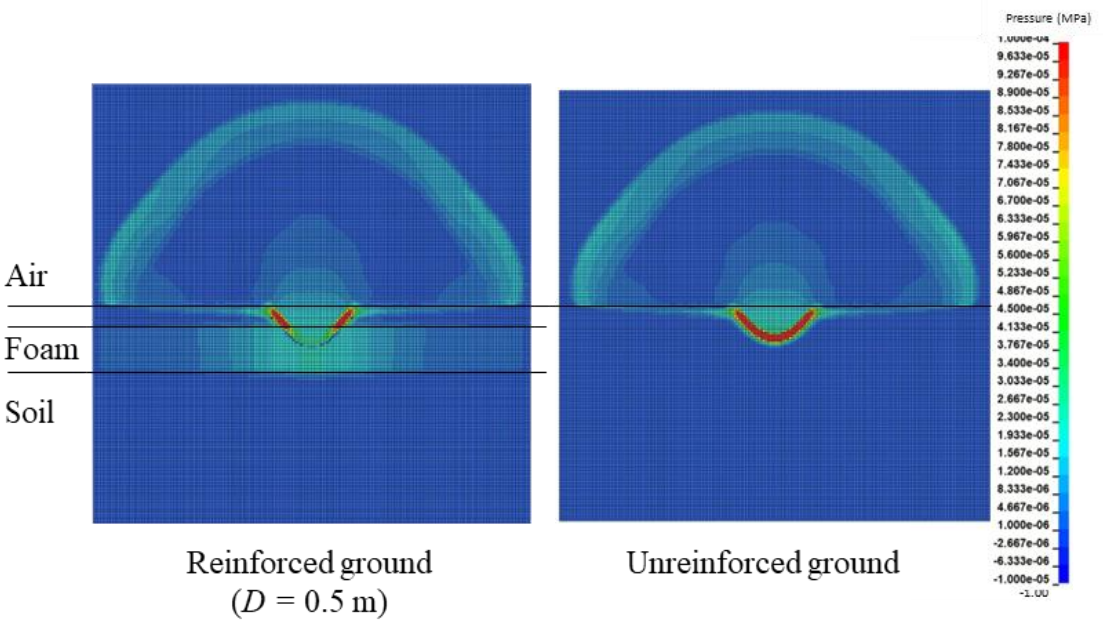

(b) t = 2 ms

doi:10.6342/NTU202401573

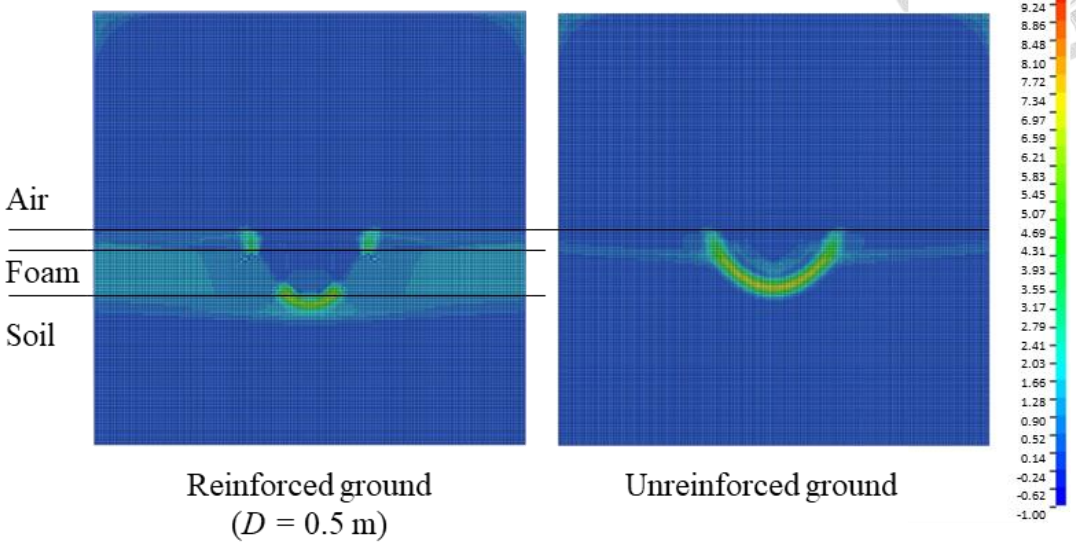

(c) t = 6 ms

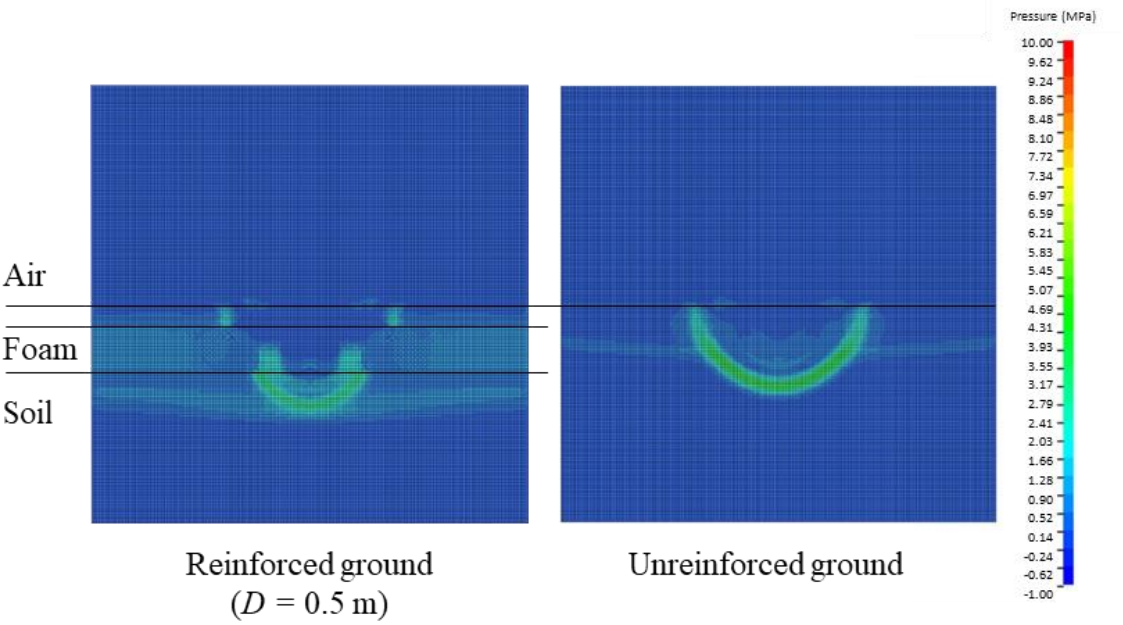

(d) t = 10 ms

doi:10.6342/NTU202401573

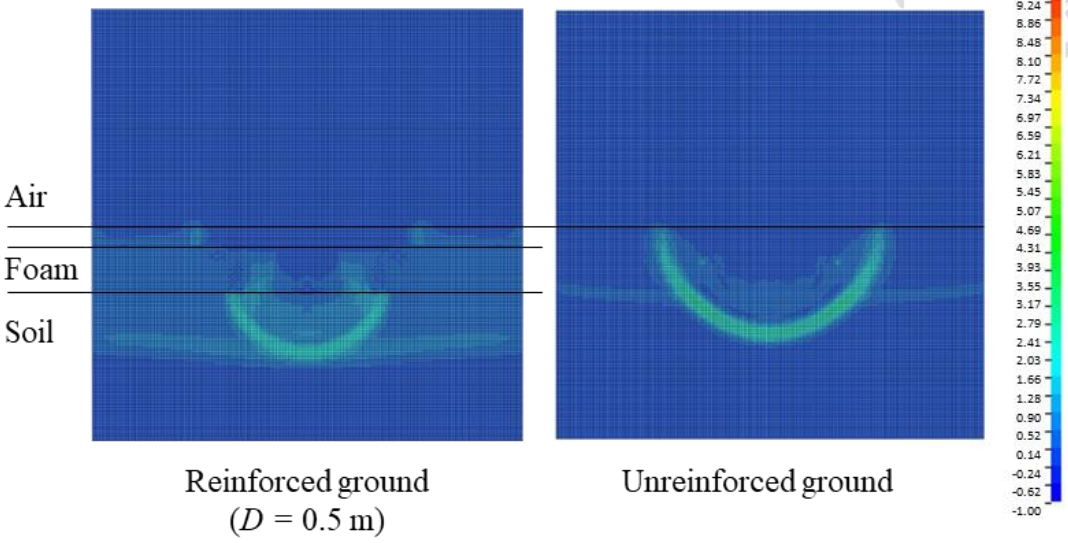

(d) t = 15 ms

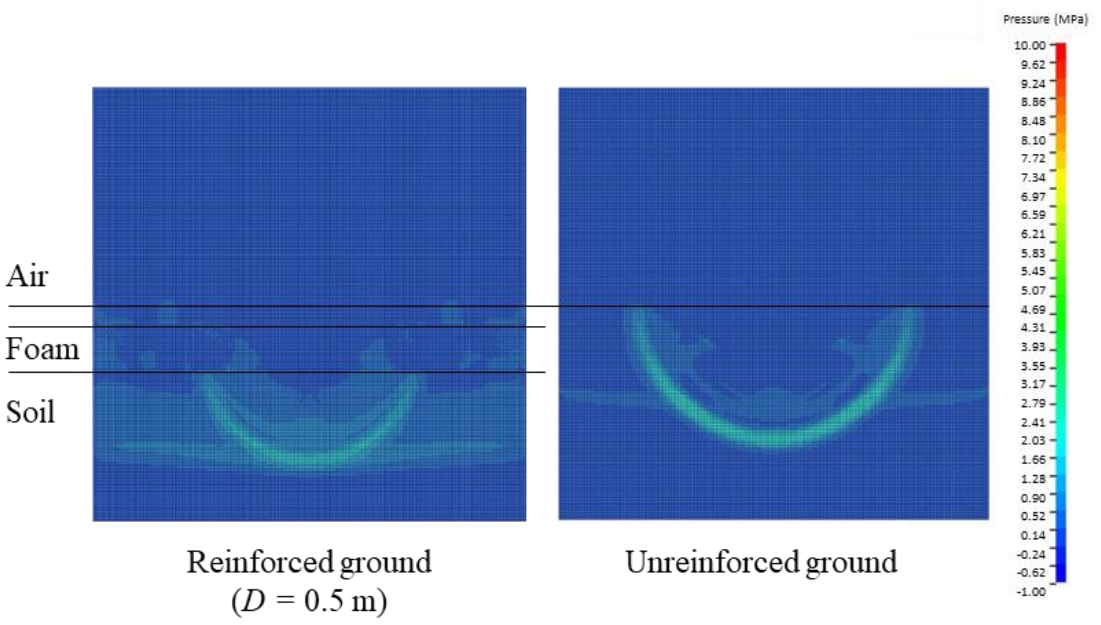

(d) t = 20 ms

Figure 5-11 Comparison of shock wave propagation in the reinforced ground (D = 0.5 m) and unreinforced ground, t = (a) 0.1 ms; (b) 2 ms; (c) 6 ms; (d) 10 ms; (e) 15 ms; (f) 20 ms

doi:10.6342/NTU202401573

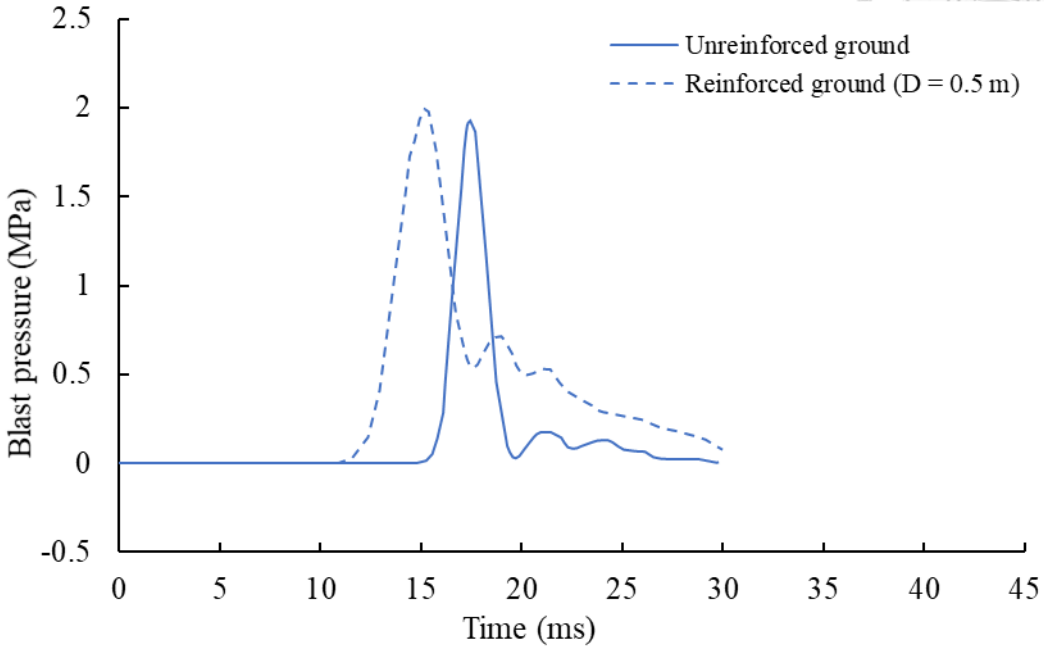

Figure 5-12 Comparison of pressure-time history between unreinforced ground and reinforced ground (D = 0.5 m)

doi:10.6342/NTU202401573

5.4. Design Recommendations

For the recommended design for a 3 m thick blast attenuation layer based on the results of parametric studies, the models with the best performance in terms of RD_b and RD_a were selected from each group of parameters. The schematic diagram for the recommended layout of the geofoam-reinforced blast attenuation layer is shown in Figure 5-13.

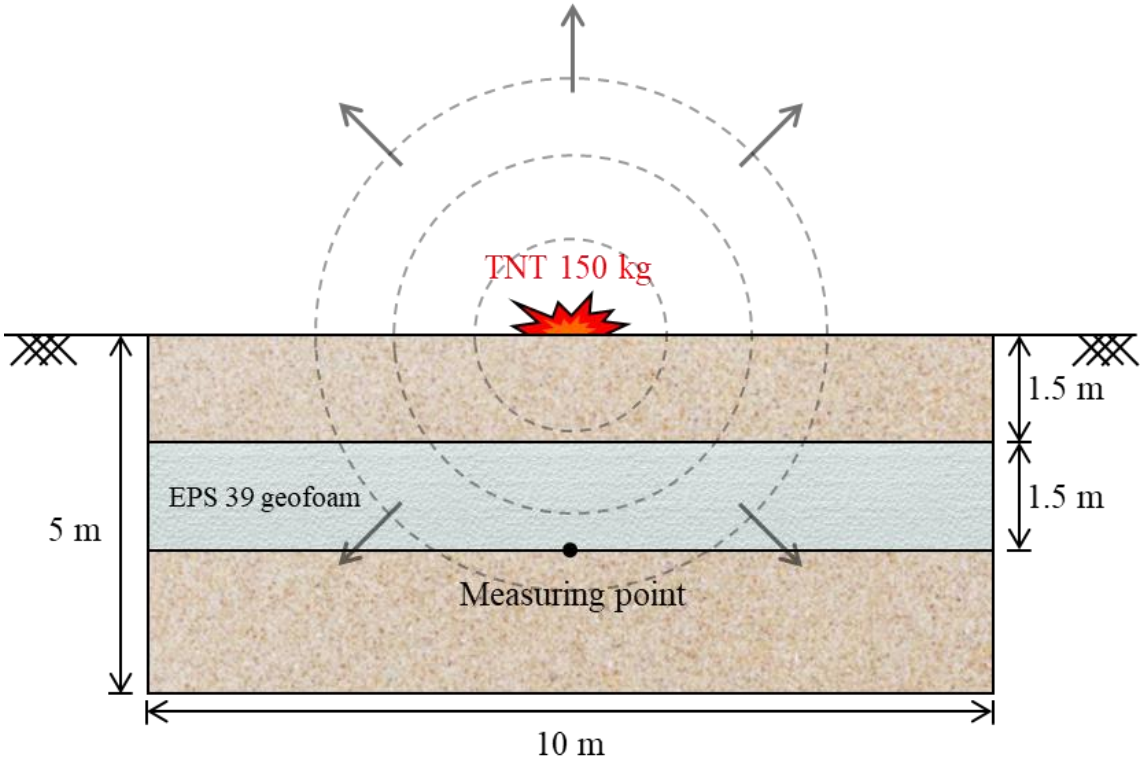

Figure 5-13 Schematic diagram for the recommended layout of geofoam-reinforced blast attenuation layer

doi:10.6342/NTU202401573

The numerical results for the recommended design are shown in Figure 5-14, Figure 5-15, as well as Table 5-6, and Table 5-7. In the numerical results of the recommended layout model, $R_b = 80.09\%$, $a_v = 98.97\%$. With the geofoam-reinforced shock wave attenuation layer, P_b is reduced to 0.384 MPa, whereas a_v is reduced to 21.916g.

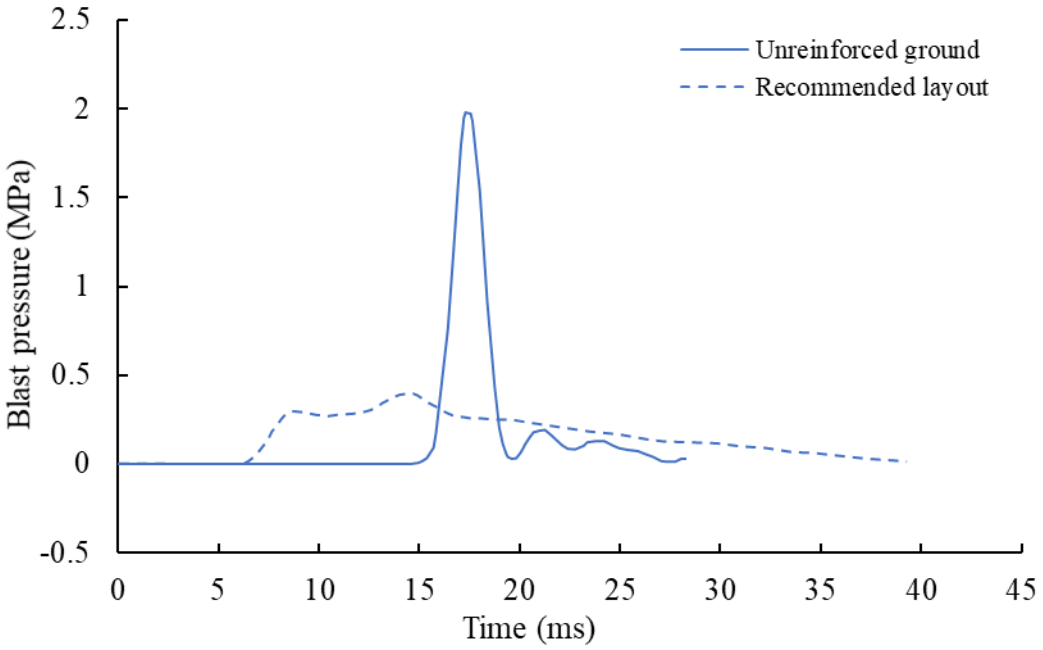

Figure 5-14 Time history of blast pressure in soil 3 m below ground surface in the recommended layout

doi:10.6342/NTU202401573

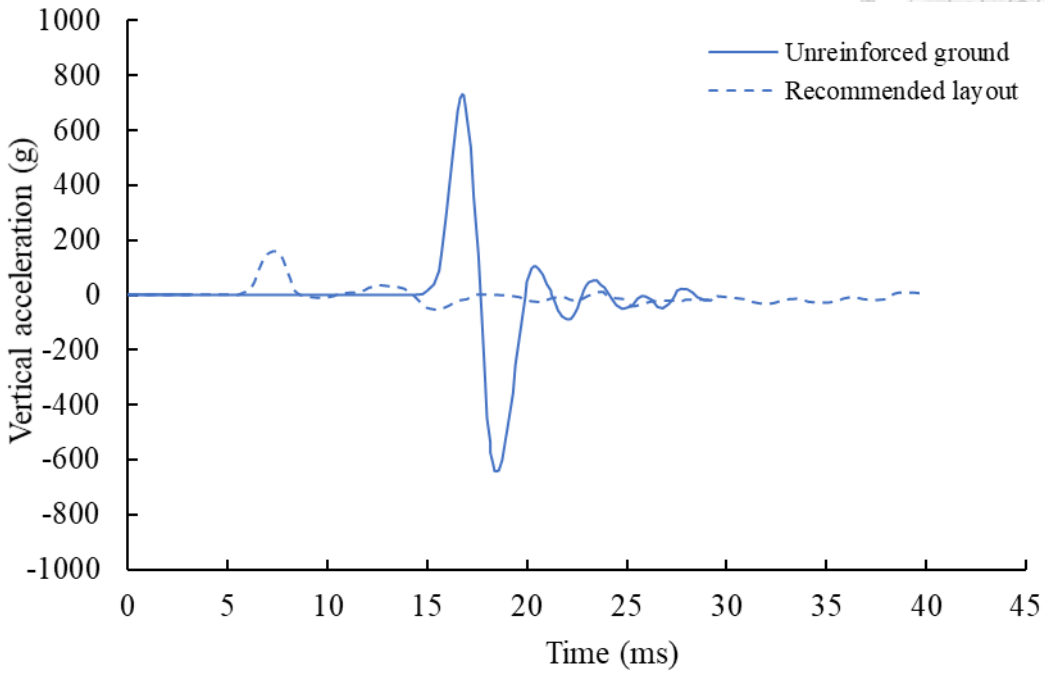

Figure 5-15 Time history of vertical acceleration in soil 3 meters below ground surface in the recommended layout

doi:10.6342/NTU202401573

doi:10.6342/NTU202401573

Table 5-6 Numerical results: reduction in peak blast pressure for each model

Parameter	EPS type	Unit weight γ (kN/m^3)	Geofoam thickness t (m)	Geofoam embedded depth D (m)	Peak blast pressure, P_b (MPa)	Reduction factor, RD_b (%)
Unreinforced ground	-	-	-	-	1.93	-
Baseline case	EPS 22	0.212	1	1	0.757	60.77
Geofoam type	EPS 39	0.384	1	1	0.567	70.6
	EPS 15	0.144	1	1	0.98	49.22
Geofoam thickness	EPS 22	0.212	1.5	1	0.47	75.64
	EPS 22	0.212	1.25	1	0.602	68.81
	EPS 22	0.212	0.75	1	1.073	44.39
	EPS 22	0.212	0.5	1	1.311	32.09
Embedded depth	EPS 22	0.212	1	1.5	0.402	79.16
	EPS 22	0.212	1	1.25	0.465	75.91
	EPS 22	0.212	1	0.75	1.483	23.15
	EPS 22	0.212	1	0.5	2.011	-4.21
Recommended layout	EPS 39	0.384	1.5	1.5	0.384	80.09

Table 5-7 Numerical results: reduction in peak vertical acceleration for each model

Parameter	EPS type	Unit weight γ (kN/m^3)	Geofoam thickness t (m)	Geofoam embedded depth D (m)	Peak vertical acceleration, a_v (g)	Reduction factor, RD_a (%)
Unreinforced ground	-	-	-	-	723.751	-
Baseline case	EPS 22	0.212	1	1	121.329	83.24
Geofoam type	EPS 39	0.384	1	1	92.836	87.17
	EPS 15	0.144	1	1	191.762	73.5
Geofoam thickness	EPS 22	0.212	1.5	1	89.849	89.85
	EPS 22	0.212	1.25	1	93.176	93.18
	EPS 22	0.212	0.75	1	71.408	71.41
	EPS 22	0.212	0.5	1	68.873	68.87
Embedded depth	EPS 22	0.212	1	1.5	32.62	95.49
	EPS 22	0.212	1	1.25	74.516	89.7
	EPS 22	0.212	1	0.75	289.501	60
	EPS 22	0.212	1	0.5	680.938	5.92
Recommended layout	EPS 39	0.384	1.5	1.5	21.916	96.97

Chapter 6. Conclusions

6.1. Conclusions

In this research, a series of numerical analyses were performed to investigate the blast-resistance mechanism and efficiency of the shock wave attenuation layer using geofoam. Based on the recommended layout for the shock wave attenuation layer proposed by the U.S. Army design manual TM5-855-1, numerical models for the shock wave attenuation layer with and without geofoam reinforcements were constructed to evaluate the performance of geofoam on reducing the blast pressure and vertical acceleration. Furthermore, a series of parametric studies were conducted to evaluate the influence of geofoam type, configuration, and embedded depth on the shock attenuation effect. The geofoam design to achieve optimal shock attenuation was identified and recommended. The conclusions of this research are shown as follows:

1. The LS-DYNA program's FHWA_SOIL model, validated through field experiments and empirical equations, is proven to accurately describe the soil's dynamic behavior under blast loads.

doi:10.6342/NTU202401573

2. The results of sensitivity studies indicate the density of geofoam is the most influential parameter, compared with bulk modulus and shear modulus, on reducing the blast pressure.

3. When 150 kg of TNT is detonated on the sandy ground surface, the numerical model predicts a peak blast pressure of 1.93 MPa at 3 m below the ground surface. The peak vertical acceleration of soil particles is predicted to be 723.751 g.

4. The numerical results indicate that when a 1 m thick EPS 22 geofoam layer embedded 1 m below ground surface is subjected to the blast load from the detonation of 150 kg of TNT, the peak blast pressure in soil at 3 m below ground surfaces is 0.757 MPa (60.77% reduction compared to the unreinforced ground), and the peak vertical acceleration of soil particle is 121.329 g (83.24% reduction compared to the unreinforced ground).

5. Parametric studies indicate that sufficient embedded depth is critical for geofoam to function as a shock wave attenuation material fully. Without sufficient embedded depth, numerical results suggest that geofoam may not effectively make use of its function, even leading to higher soil blast pressure compared to the unreinforced ground.

doi:10.6342/NTU202401573

6. For EPS 22 geofoam, the critical embedded depth is estimated to be 0.5 m. For other geofoam types, the embedded depth may vary due to the differences in the compressive resistance of each geofoam.

7. Based on parametric studies, the recommended layout for a 3 m thick shock wave attenuation layer consisting of a 1.5-meter thick EPS 39 geofoam embedded 1.5m below ground surface. The numerical model predicts the peak blast pressure in the soil is 0.384 MPa (80.09% reduction compared to the unreinforced ground) and the peak vertical acceleration of soil particles is 21.916 g (96.97% reduction compared to the unreinforced ground).

6.2. Recommendations

In this study, the performance of shock attenuation layer consisting of one soil and three geofoam types was evaluated. Future studies are recommended as follows:

1. Conduct geofoam model validation based on experimental data rather than numerical results.

2. Including underground structures in future models would help obtain structural responses and provide a more complete understanding of geofoam's effectiveness as shock wave attenuation material.

doi:10.6342/NTU202401573

3. The protection effectiveness of geofoam in varied soil conditions (e.g. clay, gravel) could be evaluated.

4. Variations in soil moisture content could be considered to evaluate the effect of soil saturation on geofoam's protection effectiveness.

5. While this research focuses on the blast attenuation effects of geofoam, future studies could use similar methods to investigate geofoam's effectiveness in reducing rockfall impacts.

doi:10.6342/NTU202401573

References

[1] 鄭卓仁(2010)，「地工泡棉運用於落石防護之模擬測試研究」，國立臺北科技大學土木與防災研究所碩士學位論文

[2] 皮盛榮(2015)，「地下指揮所近場爆炸實驗與數值模擬分析」，國防大學理工學院國防科學研究所博士學位論文

[3] 曾世傑(2022)，「以試驗與數值分析探討地工織物加勁土抵抗爆壓力之研究」，國立台灣科技大學營建工程系博士學位論文

[4] U.S.D.A. (United States Department of the Army) (1998). *Army Technical Manual No. TM 5-855-1: Design and Analysis of Hardened Structures to Convention Weapon Effects.* Headquarters Departments of the Army, the Air Force, the Navy and the Defense Special Weapons Agency, Washington, DC, USA.

[5] Wang, J. (2001). *Simulation of landmine explosion using LS-DYNA3D software: benchmark work of simulation of explosion in soil and air*. Australia: DSTO Aeronautical and Maritime Research Laboratory.

[6] USDA (2008). *Unified Facilities Criteria No. UFC 3-340-02: Structures to Resist the Effects of Accidental Explosions*. Department of the Army and Defense Special Weapons Agency, Washington, DC, USA.

[7] ASTM D6817 (2021). *Standard Specification for Rigid Cellular Polystyrene Geofoam . ASTM International*. ASTM International, West Conshohocken, PA, USA

[8] Woods, R. D. (1968). Screening of surface wave in soils. *Journal of the soil*

doi:10.6342/NTU202401573

mechanics and foundations division, *94*(4), 951-979.

[9] Horvath, J. S. (1997). The compressible inclusion function of EPS geofoam. *Geotextiles and Geomembranes*, *15*(1-3), 77-120.

[10] Reid, J. D., Coon, B. A., Lewis, B. A., Sutherland, S. H., & Murray, Y. D. (2004). *Evaluation of LS-DYNA soil material model 147* (No. FHWA-HRT-04-094). United States. Federal Highway Administration.

[11] Lee, W. Y. (2006). *Numerical modeling of blast-induced liquefaction*. Brigham Young University.

[12] Wang, Z. L., Li, Y. C., & Wang, J. G. (2006). Numerical analysis of attenuation effect of EPS geofoam on stress-waves in civil defense engineering. *Geotextiles and Geomembranes*, *24*(5), 265-273.

[13] Zarnani, S., & Bathurst, R. J. (2008). Numerical modeling of EPS seismic buffer shaking table tests. *Geotextiles and Geomembranes*, *26*(5), 371-383.

[14] Murillo, C., Thorel, L., & Caicedo, B. (2009). Ground vibration isolation with geofoam barriers: Centrifuge modeling. *Geotextiles and Geomembranes*, *27*(6), 423-434.

[15] Wang, J. G., Sun, W., & Anand, S. (2009). Numerical investigation on active isolation of ground shock by soft porous layers. *Journal of sound and vibration*, *321*(3-5), 492-509.

[16] Jayasinghe, L. B., Thambiratnam, D. P., Perera, N., & Jayasooriya, J. H. A. R. (2013). Computer simulation of underground blast response of pile in saturated soil. *Computers & Structures*, *120*, 86-95.

doi:10.6342/NTU202401573

[17] Bartlett, S. F., Lingwall, B. N., & Vaslestad, J. (2015). Methods of protecting buried pipelines and culverts in transportation infrastructure using EPS geofoam. *Geotextiles and Geomembranes*, *43*(5), 450-461.

[18] Garner, S., Strong, J., & Zavaliangos, A. (2015). The extrapolation of the Drucker–Prager/Cap material parameters to low and high relative densities. *Powder Technology*, *283*, 210-226.

[19] Barsotti, M., Sammarco, E., & Stevens, D. (2016). Comparison of strategies for landmine modeling in LS-DYNA with sandy soil material model development. In *Proceedings of 14th international LS-DYNA users conference, June* (pp. 12-14).

[20] Busch, C. L., Aimone-Martin, C. T., & Tarefder, R. A. (2016). Experimental evaluation and finite-element simulations of explosive airblast tests on clay soils. *International Journal of Geomechanics*, *16*(4), 04015097.

[21] Dubec, B., & Stonis, P. (2018). Material model parameters identification of blast environment. *Security & Future*, *2*(3), 142-145.

[22] Linforth, S., Tran, P., Rupasinghe, M., Nguyen, N., Ngo, T., Saleh, M., ... & Shanmugam, D. (2019). Unsaturated soil blast: flying plate experiment and numerical investigations. *International Journal of Impact Engineering*, *125*, 212-228.

[23] Fang, C., Yosef, T. Y., Linzell, D. G., & Rasmussen, J. D. (2021). Computational modeling and dynamic response of highway bridge columns subjected to combined vehicle collision and air blast. *Engineering Failure Analysis*, *125*, 105389.

doi:10.6342/NTU202401573

[24] Majumder, M., & Bhattacharyya, S. (2021). An alternate arrangement of geofoam blocks and air pocket to mitigate confined blast induced vibration. *International Journal of Geotechnical Engineering*, *15*(1), 52-65.

[25] Akyelken, F. A., & Kılıç, H. (2022). Experimental and numerical analyses of buried HDPE pipe with using EPS geofoam. *KSCE Journal of Civil Engineering*, *26*(9), 3968-3977.

[26] Mandal, J., Goel, M. D., & Agarwal, A. K. (2022). Study of Different Materials to Mitigate Blast Energy for the Tunnel Subjected to Buried Explosion. In *Composite Materials for Extreme Loading: Proceedings of the Indo-Korean workshop on Multi Functional Materials for Extreme Loading 2021* (pp. 505-518). Springer Singapore.

[27] Tseng, S. C., Yang, K. H., Tsai, Y. K., & Teng, F. C. (2022). Investigation of the blast-resistance performance of geotextile-reinforced soil. *Geosynthetics International*, *30*(6), 584-601.

[28] Khodaparast, M., Mohamad Momeni, R., & Bayesteh, H. (2022). Numerical simulation of surface blast reduction using composite backfill. *Geosynthetics International*, *29*(1), 66-80.

[29] Barman, R., Sarkar, A., & Bhowmik, D. (2023). Composite sand-crumb rubber and geofoam wave barrier for train vibration. *Geotechnical and Geological Engineering*, 1-23.

doi:10.6342/NTU202401573